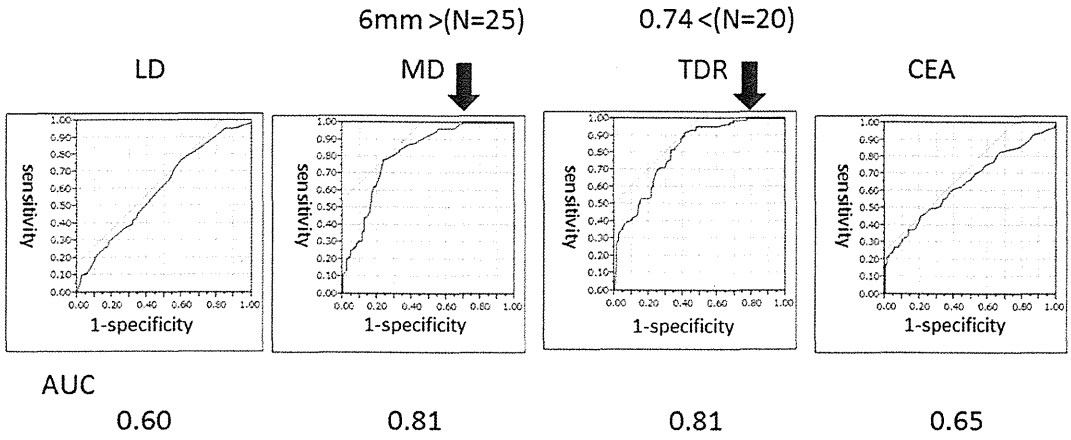

Figure 5. Receiver operating characteristic analyses for pleural, lymphatic and vascular invasion. Tumour dimension was evaluated using lung window (LD) and mediastinal window (MD) settings. TDR: tumour disappearance ratio (TDR = 1− MD/LD), CEA: carcinoembryonic antigen. Allow indicated a value at 100% sensitivity.
doi:10.1371/journal.pone.0110305.g005

In this study, the patient population was limited to those with tumour diameters of 1–3 cm. Patients with tumour diameters of < 1 cm were excluded because of the small number of cases and the major bias to perform wedge resection. Another problem was the LD and MD imaging conditions for CT. According to 7th general rule for clinical and pathological record of lung cancer, the recommended LD are a window level of −500 to −700 and a window width of 1000–2000 HU, whereas we used −500 HU and 1500 HU, respectively. The recommended MD are a window level of 30–60 H and a window width of 350–600 HU, while we used 60 HU and 350 HU, respectively.[8]

The differences in these imaging conditions for CT may have affected the MD, LD and TDR results. Furthermore, the solid component size defined as a lesion without GGO evaluated by LD is a promising method of the solid area representing an invasive lesion (scar) of the adenocarcinoma,

Therefore, further investigations on the optimal CT imaging conditions for assessing the aggressiveness of small adenocarcinomas should be performed in multiple centres with larger sample sizes. The size of the solid lesion (excluding the GGO component) evaluated using LD is also a useful CT-based prognostic factor. Further examination is necessary to clarify the relative utility of both tumour size measured using MD and extracted solid size measured by LD.

In conclusion, our results suggest that measuring tumour size with MD on high-resolution CT is a simple and useful

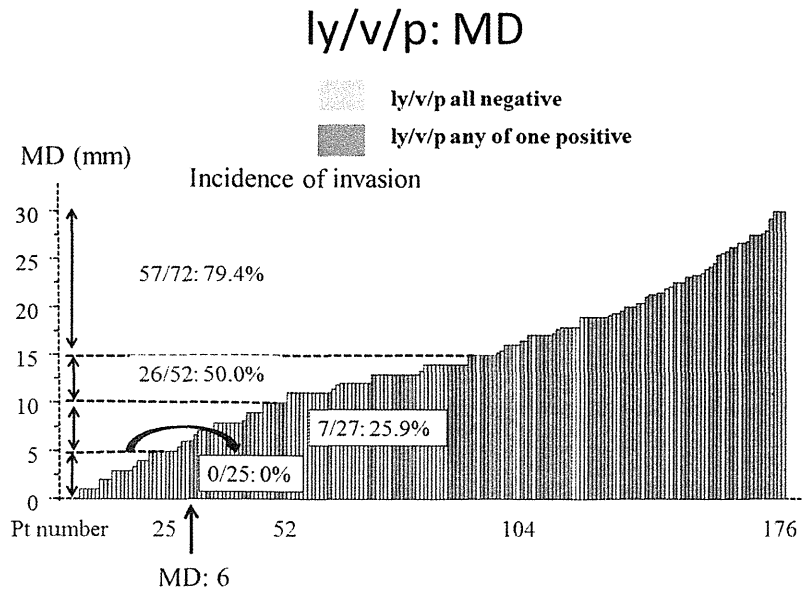

Figure 6. Incidence of lymphatic vessel, vascular vessel or pleural invasion in small adenocarcinomas according to tumour dimension using mediastinal window (MD) settings. A black bar showed a patient with invasion to any of lymphatic vessel, vascular vessel or pleura, and a gray bar showed a patient without any of them.
doi:10.1371/journal.pone.0110305.g006

preoperative modality for predicting invasiveness, lymph node metastasis and prognosis. An increased tumour size with MD correlated with pathological malignant potential reflecting tumour aggressiveness and degree of invasion.

Acknowledgments

CT imaging data and statistical advice were provided by Dr. Kuroda, Dr. Mun and Dr. Uehara. Pathological advice was given by Dr. Ishikawa and Dr. Motoi. Editorial assistance was provided by Dr. Nakagawa and Dr. Okumura.

Author Contributions

Conceived and designed the experiments: SO KN. Analyzed the data: HU HK YS. Contributed reagents/materials/analysis tools: MM YI NM. Wrote the paper: HK YS. Pathological examination and analyses (Chief of the department of pathology): YI. Pathological examination and analyses (Chief of the division of the lung pathology): NM.

References

1. Sakao Y, Nakazono T, Tomimitsu S, Takeda Y, Sakuragi T, et al. (2004) Lung adenocarcinoma can be subtyped according to tumour dimension by computed tomography mediastinal-window setting. Additional size criteria for Clinical T1 adenocarcinoma. Eur J Cardiothorac Surg 26: 1211–1215.
2. Sakao Y, Nakazono T, Sakuragi T, Natsuaki M, Itoh T (2004) Predictive factors for survival in surgically resected clinical IA peripheral adenocarcinoma of the lung. Ann Thorac Surg 77: 1157–1162.
3. Nakazono T, Sakao Y, Yamaguchi K, Imai S, Kumazoe H, et al. (2005) Subtypes of peripheral adenocarcinoma of the lung: differentiation by thin-section CT. Eur Radiol 15: 1563–1568.
4. Bhure UN, Lardinois D, Kalff V, Hany TF, Soltermann A, et al. (2010) Accuracy of CT parameters for assessment of tumour size and aggressiveness in lung adenocarcinoma with bronchoalveolar elements. Br J Radiol 83: 841–849.
5. Sakao Y, Miyamoto H, Sakuraba M, Oh T, Shiomi K, et al. (2007) Prognostic significance of a histologic subtype in small adenocarcinoma of the lung: the impact of non-bronchioloalveolar carcinoma components. Ann Thor Surg 83: 209–214.
6. Travis WD, Brambilla E, Noguchi M, Nicholson AG, Geisinger KR, et al. (2011) International Association for the Study of Lung Cancer/American Thoracic Society/European Respiratory Society International Multidisciplinary Classification of Lung Adenocarcinoma. J Thorac Oncol 6: 244–285.
7. Shimosato Y, Suzuki A, Hashimoto T, Nishiwaki Y, Kodama T, et al. (1980) Prognostic implications of fibrotic focus (scar) in small peripheral lung cancers. Am J Sur g Pathol 4: 365–373.
8. Rusch VW, Asamura H, Watanabe H, Giroux DJ, Rami-Porta R, et al. (2009) The IASLC lung cancer staging project: a proposal for a new international lymph node map in the forthcoming seventh edition of the TNM classification for lung cancer. J Thorac Oncol 4: 568–577.
9. Maeshima AM, Niki T, Maeshima A, Yamada T, Kondo H, et al. (2002) Modified scar grade: a prognostic indicator in small peripheral lung adenocarcinoma. Cancer 95: 2546–54.
10. Borczuk AC, Qian F, Kazeros A, Eleazar J, Assaad A, et al. (2009) Invasive size is an independent predictor of survival in pulmonary adenocarcinoma. Am J Surg Pathol 33: 462–469.
11. Noguchi M, Morikawa A, Kawasaki M, Matsuno Y, Yamada T, et al. (1995) Small adenocarcinoma of the lung. Histologic characteristics and prognosis. Cancer 75: 2844–2852.
12. Kulpa J, Wo'jcik E, Reinfuss M, Kolodziejski L (2002) Carcinoembryonic antigen, squamous cell carcinoma antigen, CYFRA21-1, and neuron-specific enolase in squamous cell lung cancer patients. Clin Chem 48: 1931–1937.
13. Sawabata N, Maeda H, Yokota S, Takeda S, Koma M, et al. (2004) Postoperative serum carcinoembryonic antigen levels in patients with pathologic stage IA nonsmall cell lung carcinoma: subnormal levels as an indicator of favorable prognosis. Cancer 15: 803–809.
14. Sakao Y, Sakuragi T, Natsuaki M, Itoh T (2003) Clinicopathological analysis of prognostic factors in clinical IA peripheral adenocarcinoma of the lung. Ann Thorac Surg 75: 1113–1117.
15. Suzuki K, Koike T, Asakawa T, Kusumoto M, Asamura H, et al. (2011) A prospective radiological study of thin-section computed tomography to predict pathological noninvasiveness in peripheral clinical IA lung cancer (Japan Clinical Oncology Group 0201). J Thorac Oncol 6: 751–756.
16. Okada M, Nishio W, Sakamoto T, Uchino K, Hanioka K, et.al. (2004) Correlation between computed tomographic findings, bronchioloalveolar carcinoma component, and biologic behavior of small-sized lung adenocarcinomas. J Thorac Cardiovasc Sur 127: 857–861.
17. Takashima S, Maruyama Y, Hasegawa M, Yamanda T, Honda T, et al. (2002) Prognostic significance of high-resolution CT findings in small peripheral adenocarcinoma of the lung: a retrospective study on 64 patients. Lung Cancer 36: 289–295.

A Novel Mechanism of *EML4-ALK* Rearrangement Mediated by Chromothripsis in a Patient-Derived Cell Line

Tatsushi Kodama, MS, Noriko Motoi, MD, PhD,†§ Hironori Ninomiya, MD, PhD,†§ Hiroshi Sakamoto, PhD,* Kunio Kitada, PhD,* Toshiyuki Tsukaguchi, MS,* Yasuko Satoh, DVM,* Kimie Nomura, MS,† Hiroko Nagano, MS,† Nobuya Ishii, PhD,* Yasuhito Terui, MD, PhD,‡ Kiyohiko Hatake, MD, PhD,‡ and Yuichi Ishikawa, MD, PhD,†§*

Introduction: *EML4-ALK* is a driver oncogene in non–small-cell lung cancer (NSCLC) and has been developed into a promising molecular target for antitumor agents. Although *EML4-ALK* is reported to be formed by inversion of chromosome 2, other mechanisms of this gene fusion remain unknown. This study aimed to examine the mechanism of *EML4-ALK* rearrangement using a novel cell line with the *EML4-ALK* fusion gene.

Methods: An *EML4-ALK*-positive cell line, termed JFCR-LC649, was established from pleomorphic carcinoma, a rare subtype of NSCLC. We investigated the chromosomal aberrations using fluorescence in situ hybridization and comparative genomic hybridization (CGH). Alectinib/CH5424802, a selective ALK inhibitor, was evaluated in the antitumor activity against JFCR-LC649 in vitro and in vivo xenograft model.

Results: We established an *EML4-ALK*-positive cell line, termed JFCR-LC649, derived from a patient with NSCLC and revealed that the JFCR-LC649 cells harbor variant 3 of the *EML4-ALK* fusion with twofold copy number gain. Interestingly, comparative genomic hybridization and metaphase-fluorescence in situ hybridization analysis showed that in addition to two normal chromosome 2, JFCR-LC649 cells contained two aberrant chromosome 2 that were fragmented and scattered. These observations provided the first evidence that *EML4-ALK* fusion in JFCR-LC649 cells was formed in chromosome 2 by a distinct mechanism of genomic rearrangement, termed chromothripsis. Furthermore, a selective ALK inhibitor alectinib/CH5424802 suppressed tumor growth of the JFCR-LC649 cells through inhibition of phospho-ALK in vitro and in vivo in a xenograft model.

Conclusion: Our results suggested that chromothripsis may be a mechanism of oncogenic rearrangement of *EML4-ALK*. In addition, alectinib was effective against *EML4-ALK*-positive tumors with *ALK* copy number gain mediated by chromothripsis.

Key Words: ALK, Lung cancer, Chromosomal rearrangement, Chromothripsis, ALK inhibitor.

(*J Thorac Oncol.* 2014;9: 1638–1646)

Tyrosine kinase fusion genes have been identified in some cancers, and the constitutive activation of these fusion kinases is involved in tumorigenesis. *BCR-ABL* fusion gene was found in chronic myelogenous leukemia, and the ABL inhibitor imatinib is a successful drug for chronic myelogenous leukemia patients.[1] In addition to *BCR-ABL*, the *ALK*, *ROS1*, and *RET* fusion genes have recently been identified as driver oncogenes in non–small-cell lung cancer (NSCLC).[2–5] The tumorigenic potential of these fusion genes, namely *EML4-ALK*, *CD74-ROS1*, and *KIF5B-RET*, was confirmed using a transformation assay via subcutaneous injection of the transfected 3T3 cells into nude mice.[2,3] Of those, patients with *ALK* fusion-positive NSCLC have responded in clinic to treatment with ALK inhibitors.[6–8] In addition, crizotinib has recently demonstrated its efficacy in the treatment of NSCLC with *ROS1* translocations.[9] Furthermore, in a prospective phase 2 trial that included *RET* fusion-positive NSCLC patients, two patients with *RET* fusion-positive NSCLC responded to cabozantinib.[10] Thus, fusion genes are considered to be promising targets for anticancer therapy.

Most of the fusion genes are generated by chromosomal rearrangements, such as translocation or inversion. Although the genetic alterations in tumorigenesis can accumulate gradually over time, a recent study has revealed a new phenomenon in which tens to hundreds of chromosomal rearrangements are acquired simultaneously by a single catastrophic event.[11] This phenomenon, termed chromothripsis, can be seen in at least 2 to 3% of all cancers and is often believed to promote tumorigenesis in a wide variety of tumors: indeed, chromothripsis is associated with a more aggressive clinical course in neuroblastoma, multiple myeloma, colorectal cancer, and medulloblastoma.[12–15] Chromothripsis may result in chromosomal rearrangement and copy number changes, including deletion of tumor suppressor genes and amplification of oncogenes. In one neuroblastoma tumor, chromothripsis resulted in

*Research Division, Chugai Pharmaceutical Co., Ltd., Kamakura, Japan; †Division of Pathology, The Cancer Institute; ‡Division of Clinical Chemotherapy, Cancer Chemotherapy Center, Japanese Foundation for Cancer Research; and §Department of Pathology, The Cancer Institute Hospital, Tokyo, Japan.

T.K. and N.M. contributed equally to this study.

Disclosure: T.K., H.S., K.K., T.T., Y.S., and N.I. are employees of Chugai Pharmaceutical Co., Ltd. K.H. and Y.I. received research grants from Chugai Pharmaceutical Co., Ltd. All other authors declare no conflict of interest.

Address for correspondence: Hiroshi Sakamoto, Research Division, Chugai Pharmaceutical Co., Ltd., 200 Kajiwara, Kamakura, Kanagawa 247-8530, Japan. E-mail: sakamotohrs@chugai-pharm.co.jp

DOI: 10.1097/JTO.0000000000000311

ISSN: 1556-0864/14/0911-1638

amplification and very strong overexpression of c-Myc.[12] In addition, two different medulloblastoma tumors have translocation of *PVT1*, including *PVT1-MYC* and *PVT1-NDRG*, that arose via chromothripsis.[16]

EML4-ALK results from a small inversion within chromosome 2p, which leads to the expression of a chimeric tyrosine kinase, in which the N-terminus of EML4 is fused to the intracellular kinase domain of ALK.[2] However, the detailed mechanisms of *EML4-ALK* rearrangement remain unknown. Here, we explore the mechanism of *EML4-ALK* rearrangement using a novel cell line with the *EML4-ALK* fusion gene, considering a potential role of chromothripsis for the fusion formation.

PATIENTS AND METHODS

Compounds and Cell Lines

Alectinib/CH5424802 was synthesized at Chugai Pharmaceutical Co., Ltd. according to the procedure described in patent publication WO2010143664. Crizotinib was purchased from Selleck Chemicals (Houston, TX) and gefitinib was purchased from Kemprotec Limited (Lancashire, UK) JFCR-LC649 cells were established at the Japanese Foundation for Cancer Research (JFCR) from a treatment-naive female NSCLC patient. NCI-H2228 and NCI-H522 cells were obtained from American Type Culture Collection (Rockville, MD). Generation of Ba/F3 cells expressing EML4-ALK was described in our previous study.[17] This study was approved by the research ethics committees of both JFCR and Chugai Pharmaceutical Co. Ltd.

RT-PCR and Direct Sequence

Total RNA was extracted using the RNeasy kit (Qiagen, Hilden, Germany), and reverse-transcriptase polymerase chain reaction (RT-PCR) analysis was performed with sets of primers (Supplementary Table 1, Supplemental Digital Content, http://links.lww.com/JTO/A678) to detect the *EML4-ALK* variant. Direct sequence was done with ABI Prism 3100 Genetic Analyzer (Applied Biosystems, Foster City, CA).

Fluorescent In Situ Hybridization

For *ALK* break-apart fluorescent in situ hybridization (FISH) experiments, formalin-fixed paraffin-embedded (FFPE) 4-μm sections of JFCR-LC649 xenograft tumors were deparaffinized and treated with Pretreatment Reagent (Abbott Molecular, Inc., Des Plaines, IL) at 80°C for 10 minutes and then with pepsin solution (Zytovision, Bremerhaven, Germany) at 37°C for 10 minutes. Vysis LSI ALK Dual Color, Break Apart Rearrangement Probe (Abbott Molecular, Inc.) was applied to detect *ALK* gene rearrangement. Slides and probes were denatured simultaneously at 75°C for 10 minutes, followed by hybridizing at 37°C overnight with Thermobrite (Abbott Molecular, Inc.). After stringent washing with 0.3% NP-40/2× SSC at 72°C for 2 minutes, slides were mounted with DAPI (Life Technologies, Grand Island, NY). For metaphase probe-FISH analysis, JFCR-LC649 cells were incubated with Colcemid (Life Technologies) overnight at 37°C. Cells were trypsinized and a hypotonic treatment was performed. Fixation was performed in Carnoy's fixative, and this suspension was spread onto glass slides. Slides were denatured in 2× SSC/70% formamide at 68°C for 3 minutes, dehydrated through 70%, 90%, and 100% ethanol, and air-dried. FISH probes were denatured at 75°C for 10 minutes and applied onto slides, and then hybridized at 37°C overnight. Slides were washed and mounted with DAPI. Hybridization signals were captured with a fluorescence microscope (Eclipse E600; Nikon, Tokyo, Japan) equipped with appropriate filter sets. The 3′ *ALK* gene probe labeled with fluorescein isothiocyanate (GSP Laboratory, Kanagawa, Japan) was used in combination with a probe for the centromeric region of chromosome 2 labeled with SpectrumOrange (Abbott Molecular, Inc.). Metaphase probe-FISH analysis to verify the evidence of chromothripsis was performed as previously described.[18] FISH probes were generated from DNA fragments that were amplified by PCR using 3 primer pairs covering a sequence region of up to 30 kb in size within a segment. The probe information is described in Supplementary Table S2 (Supplemental Digital Content, http://links.lww.com/JTO/A678). These DNA fragments were labeled with biotin-16-dUTP or digoxigenin-11-dUTP using a labeling reagent for array-comparative genomic hybridization (CGH) analysis (Agilent Biosystems, Santa Clara, CA) and used for hybridization. Hybridization signals were detected by avidin-fluorescein (Roche Applied Science, Indianapolis, IN) and fluorescein anti-avidin antibody (Vector Laboratories, Burlingame, CA) for biotin-labeled probes and anti-digoxigenin antibody (Roche Applied Science, Indianapolis, IN) and Alexa 568 anti-mouse IgG (Molecular Probes, Eugene, OR) for digoxigenin-labeled probes. The images were recorded using a fluorescence microscope (Eclipse E600; Nikon) equipped with a digital camera (Ds-Ri1-U2; Nikon).

Immunohistochemistry

ALK immunohistochemistry (IHC) was performed with an ALK detection kit (Nichirei Biosciences, Inc., Tokyo, Japan). NSCLC cell lines were cultured on chamber slides (Iwaki, Chiba, Japan), fixed with cold 70% ethanol, permeabilized with 0.2% Triton X100/PBS, and used following the manufacturer's procedure. Briefly, pre-diluted ALK mouse monoclonal antibody, 5A4 was applied and incubated for 30 minutes at room temperature. After using a bridge reagent to amplify the signal horseradish peroxidase linked antibody and 3,3′-diaminobenzidine tetrahydrochloride were used for detection. Positivity in the culture cell image is recognized by brown staining compared with negative control, which did not show any irrelevant background staining.

FFPE 4-μm sections of JFCR-LC649 xenograft tumors were depleted of paraffin with xylene, rehydrated through a graded series of ethanol solutions, and subjected to immunohistochemical staining with a mouse monoclonal antibody of Napsin A (IP64, Novocastra, Newcastle, UK), E-cadherin (NCH-38, Dako, Glostrup, Denmark), vimentin (V9, Dako), or TTF-1 (8G7G3/1, Dako) or with a rabbit polyclonal antibody of p40 (5-17, Calbiochem, Billerica, MA). Heat-induced antigen retrieval pretreatment was performed with Bond Epitope Retrieval solution 2 pH 9.0 (Leica, Newcastle, UK).

Array-Based Comparative Genomic Hybridization

The PCR-amplified DNA and the control DNA were separately labeled with Cy5-dUTP and Cy3-dUTP, respectively,

then mixed and hybridized to human genome 244K standard microarrays or SurePrint G3 human CGH arrays containing 974,000 probes (Agilent Technologies) according to the manufacturer's protocol. The procedure for labeling of DNA and hybridization to microarrays is described in the manufacturer's instructions. Fold changes in the hybridization signal intensities of sample genomic DNA relative to the normal genomic DNA were visualized using Genomic Workbench software (Agilent Technologies) and SignalMap software (Nimblegen Systems, Inc., Madison, WI).

Cell Growth Inhibition and Caspase-3/7 Assay

Cells were cultured in 96-well spheroid plates (Sumilon Celltight Spheroid 96U; Sumitomo Bakelite, Inc., Tokyo, Japan) overnight and incubated with various concentrations of compound for the indicated time. The viable cells were measured by the CellTiter-Glo luminescent cell viability assay (Promega, Fitchburg, WI). Caspase-3/7 assay was evaluated using the Caspase-Glo 3/7 Assay Kit (Promega). Fluorescence was quantified using Envision (PerkinElmer, Waltham, MA).

Immunoblotting and Immunoprecipitation

Cells were lysed in Cell Lysis Buffer (Cell Signaling Technology) containing 1 mM PMSF, 1% (v/v) phosphate inhibitor cocktail 1 (Sigma-Aldrich, St. Louis, MO), 1% (v/v) phosphate inhibitor cocktail 2 (Sigma), and Complete Mini, EDTA-Free 1 (Roche Applied Science). Cell lysates were subjected to sodium dodecyl sulfate-polyacrylamide gel electrophoresis, and the separated proteins were electrophoretically transferred to Immobilon-P membranes (Millipore). After blocking in Blocking One (Nacalai Tesque, Inc.), the membranes were incubated independently in the primary antibodies diluted with anti-ALK (Life Technologies, #51-3900), anti-STAT3 (Cell Signaling Technology, #9132; Cell Signaling Technologies, Danvers, MA), anti-Phospho-STAT3 (Tyr 705; Cell Signaling Technology, #9131), anti-AKT (Cell Signaling Technology, #9277), anti-Phospho-AKT (Ser 473; Cell Signaling Technology, #9271), anti-p44/42 MAP Kinase (ERK1/2; Cell Signaling Technology, #9102), or anti-Phospho-ERK1/2 (Thr 202/Tyr 204; Cell Signaling Technology, #9101). To detect phosphorylated ALK, cell lysates were immunoprecipitated with anti-phosphotyrosine (PY-20) antibody (BD Biosciences, San Jose, CA). The immunoprecipitants were then collected with Protein G sepharose (GE Healthcare, Waukesha, WI) and subjected to immunoblot analysis using an anti-ALK antibody. The membranes were incubated with an anti-rabbit HRP-linked antibody (Cell Signaling Technology). The bands were detected with ECL-plus (GE Healthcare) or Chemi-Lumi One Super (Nacalai Tesque, Inc.) followed by LAS-4000 (Fujifilm, Tokyo, Japan).

In Vivo Studies

Cell lines were used to evaluate the antitumor activity of alectinib in vivo. They were grown as subcutaneous tumors in SCID mice (CLEA Japan, Inc., Tokyo, Japan) that were then randomized to treatment groups to receive vehicle or alectinib (oral, qd) for the indicated duration. Final concentration of vehicle was 0.02N HCl, 10% DMSO, 10% Cremophor EL, 15% PEG400, and 15% HPCD (2-hydroxypropyl-β-cyclodextrin). The length (L) and width (W) of the tumor mass were measured, and the tumor volume (TV) was calculated as: $TV = (L \times W^2)/2$. Tumor growth inhibition was calculated using the following formula: Tumor growth inhibition = $[1 - (T - T_0)/(C - C_0)] \times 100$, where T and T_0 are the mean tumor volumes on a specific experimental day and on the first day of treatment, respectively, for the experimental groups and likewise, where C and C_0 are the mean tumor volumes for the control group. The rate of change in body weight (BW) was calculated using the following formula: $BW = W/W_0 \times 100$, where W and W_0 are the body weight on a specific experimental day and on the first day of treatment, respectively. All animal experiments in this study were performed in accordance with protocols approved by the Institutional Animal Care and Use Committee (IACUC) of Chugai Pharmaceutical Co., Ltd.

RESULTS

Characterization of the Novel *EML4-ALK*-Positive NSCLC Cell Line

We established a novel cell line, termed JFCR-LC649, which was derived from an ALK-positive, chemotherapy-naive, female NSCLC patient, who had never smoked. First, we conducted IHC on mouse xenograft tumors of JFCR-LC649 cells to detect the expression of TTF-1 and Napsin A (as markers of type II pneumocytes),[19,20] vimentin (as a marker of mesenchymal cells),[21,22] E-cadherin (as a marker of epithelial cells),[21,22] and p40 (as a marker of basal cells or squamous cell carcinoma).[23] From these stainings, we found that the xenograft tumors were positive for TTF-1, Napsin A, vimentin, and E-cadherin but negative for p40 (Supplementary Figure S1, Supplemental Digital Content, http://links.lww.com/JTO/A678), indicating that JFCR-LC649 cells were associated with a phenotype characterized by lung adenocarcinoma cells undergoing epithelial–mesenchymal transition.

Next, to determine ALK status in JFCR-LC649 cells, we performed ALK IHC analysis and RT-PCR analysis. ALK IHC analysis confirmed that JFCR-LC649 cells expressed ALK protein (Fig. 1*A*), and RT-PCR analysis showed that they have *EML4-ALK* variant 3, which is exactly the same *EML4-ALK* variant as in NCI-H2228 (Fig. 1*B*, Supplementary Figure S2*A*, Supplemental Digital Content, http://links.lww.com/JTO/A678). Sequencing of the JFCR-LC649 transcript showed that it was the product of *EML4-ALK* variant 3, and that there were no mutations of the ALK kinase domain (Supplementary Figure S2*B*, Supplemental Digital Content, http://links.lww.com/JTO/A678).

Furthermore, we performed *ALK* break-apart FISH assays to confirm the chromosomal rearrangement in JFCR-LC649 cells. Interestingly, JFCR-LC649 cells have twofold *ALK* copy number gain compared with conventional cytogenetics, as well as the *EML4-ALK* fusion gene (Fig. 1*C*). From 244K array-based CGH analysis, we confirmed that JFCR-LC649 cells have a twofold *ALK* copy number gain compared with normal cells and, in addition, have an extremely unusual pattern of allelic changes or "allele number oscillation" in chromosome 2, on which *ALK* is located (Fig. 1*D*, Supplementary Figures S3 and S4, Supplemental Digital Content, http://links.

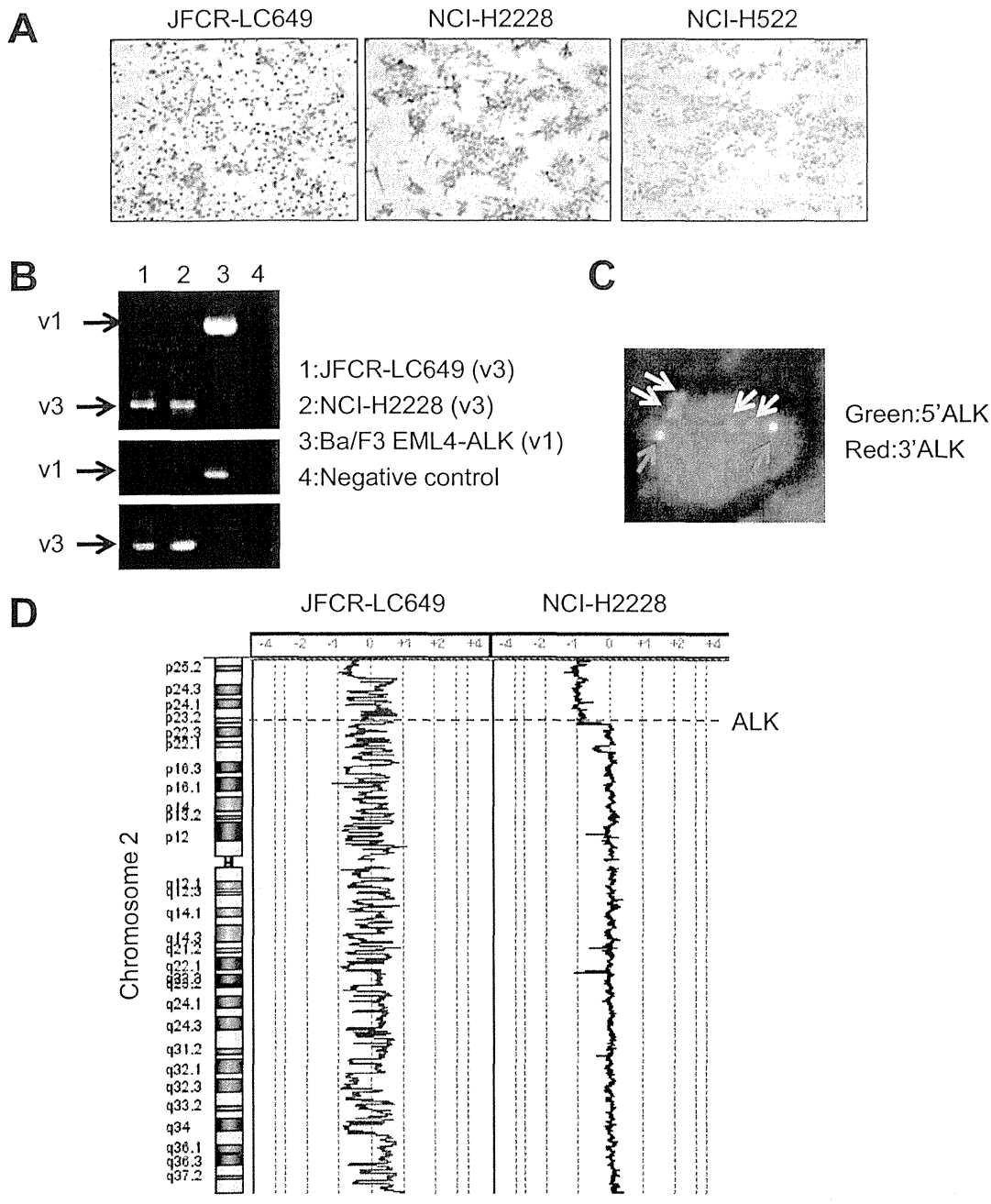

FIGURE 1. Characterization of patient-derived cell line JFCR-LC649. *A*, In IHC analysis for ALK, both JFCR-LC649 and NCI-H2228 cells were positive for ALK. NCI-H522 cells were used as a negative control. *B*, In *EML4-ALK* fusion-specific RT-PCR, JFCR-LC649 cells expressed EML4-ALK variant 3. NCI-H2228 cells harboring EML4-ALK variant 3, Ba/F3 cells transfectant EML4-ALK variant 1, and water as a negative control were used. *C*, In the *ALK* break-apart FISH assay, separate *3′ALK* signals (red) and *5′ALK* signals (green) individually existed, indicating that JFCR-LC649 cells harbored *ALK* rearrangement. JFCR-LC649 cells contained two *ALK* fusion-positive chromosome 2 (indicated with yellow arrows) and two *ALK* fusion-negative chromosome 2 (indicated with red arrows). *D*, 244K array-based CGH analysis shows the ALK copy number gain and distinct chromosomal pattern in chromosome 2 of JFCR-LC649 cells.

lww.com/JTO/A678). On the other hand, another EML4-ALK-positive cell line, NCI-H2228, does not have this unique chromosome 2 (Fig. 1*D*). In addition, a good concordance of copy number profile for chromosome 2 between JFCR-LC649 cells and the corresponding original tumor materials was observed (Supplementary Figure S5, Supplemental Digital Content, http://links.lww.com/JTO/A678). Such a phenomenon can be seen in the specific chromosomal loci in some

clinical samples and in cell lines involved in a one-off catastrophic event termed chromothripsis.[11–15,24] Thus, this unique chromosome 2 of JFCR-LC649 cells could correspond to the phenomenon of chromothripsis.

EML4-ALK Rearrangement Mediated by Chromothripsis in JFCR-LC649

Chromothripsis is a phenomenon in which tens to hundreds of chromosomal rearrangements can be generated simultaneously via a single catastrophic event. Stephens et al.[11] describe that the number of copy number states within the areas caused by chromothripsis oscillates between one and two (and occasionally three). To verify whether JFCR-LC649 cells harbor this hallmark of chromothripsis, we conducted 1M array-based CGH analysis (high-resolution array-CGH analysis). Within chromosome 2 of JFCR-LC649 cells, an oscillating pattern between two copy number states was recapitulated (Fig. 2*A*), suggesting that JFCR-LC649 cells harbor chromothripsis-derived characteristic chromosome 2.

To confirm that chromosome 2 of JFCR-LC649 cells were mediated by chromothripsis, we examined metaphase chromosome spread from JFCR-LC649 cells that was analyzed using a 3′*ALK* probe in combination with the probe for the centromeric region of chromosome 2 to understand the number and size of chromosome 2. We found that, in addition to two normal chromosome 2, JFCR-LC649 cells contained two aberrant chromosome 2, that were shorter than the length of its normal chromosome 2 (Fig. 2*B*). On the other hand, normal lymphocytes contained two normal chromosome 2 (Supplementary Figure S6, Supplemental Digital Content, http://links.lww.com/JTO/A678). These data were similar to a previous report that TK10 (a renal cancer cell line) with genomic landscapes harboring the hallmarks of chromothripsis showed four grossly normal copies of chromosome 5 and two smaller derivative chromosomes.[11] To further understand the aberrant chromosome 2 in JFCR-LC649 cells, we conducted metaphase-FISH analysis using a probe with a red signal and 2 different kinds of probes with green signals designed by using the data from the 1M array-based CGH analysis (Fig. 2*D*). These probe sets target adjacent regions of the genome in normal chromosome 2. All signals existed in the same positions in normal chromosome 2, but the green signals split in aberrant chromosome 2, indicating that fragmentation and scattering of the chromosome had occurred (Fig. 2*C*).[11] These results indicated that the aberrant chromosomes were generated by chromothripsis. Thus, these observations provide us the first evidence that *EML4-ALK* in chromosome 2 of JFCR-LC649 cells was mediated by chromothripsis (Fig. 3).

Potency of ALK Inhibitor Alectinib Against JFCR-LC649 Cells with *ALK* Copy Number Gain

Previous reports showed that copy number gain of *EML4-ALK* has been observed both in cell lines and in patient tumors as an additional mechanism of crizotinib resistance in ALK-positive NSCLC.[25,26] To clarify the sensitivity to ALK inhibitors against the cell lines with *ALK* copy number gain, we tested the cell growth inhibitory effect of a selective ALK inhibitor alectinib,[17] or crizotinib against JFCR-LC649 cells. Alectinib and crizotinib both inhibited the cell growth of JFCR-LC649 cells, and the potency of alectinib was approximately 13-fold more potent than that of crizotinib (Fig. 4*A*). On the other hand, an EGFR inhibitor gefitinib did not inhibit its growth (Fig. 4*A*). In addition, alectinib induced caspase-3/7 activation in JFCR-LC649 cells (Fig. 4*B*), indicating that apoptosis induction is involved in the antitumor activity of alectinib. To understand the effect of phospho-ALK suppression and the contribution of ALK downstream components, we conducted a cellular phosphorylation assay using JFCR-LC649 cells that had been treated with alectinib. Alectinib suppressed auto-phosphorylation of ALK in a concentration-dependent manner (Fig. 4*C*). In addition, alectinib also suppressed phosphorylation of STAT3 but did not suppress phosphorylation of AKT and ERK1/2 (Fig. 4*C*). The inhibitory activity on phospho-STAT3 and the apoptosis-inducing activity of crizotinib are weaker than those of alectinib (Supplementary Figure S7*A*, *B*, Supplemental Digital Content, http://links.lww.com/JTO/A678).

We next tested the efficacy of alectinib and crizotinib in a mouse xenograft model of JFCR-LC649 cells. Although the engraftment of JFCR-LC649 cells took a long time, IHC analysis showed that JFCR-LC649 xenograft tumors still expressed ALK protein 101 days after the inoculation (Fig. 5*A*). Using this xenograft model, we confirmed that once-daily oral administration of alectinib resulted in remarkable tumor regression at all dose levels ($p < 0.001$, alectinib versus vehicle treatment using parametric Dunnett's test) without significant body weight loss (Fig. 5*B*) and its nearly equal activity against another EML4-ALK-positive cell line, NCI-H2228, has already been observed.[17] Crizotinib at the maximum tolerated dose (MTD: 100 mg/kg) in mice[27] also resulted in remarkable tumor regression against JFCR-LC649 bearing mice models (Fig. 5*B*). In the phosphorylation assay of the JFCR-LC649 xenograft tumors, both alectinib and crizotinib suppressed auto-phosphorylation of ALK in vivo (Fig. 5*C*). Taken together, we confirmed both in vitro and in vivo in a xenograft model that both alectinib and crizotinib were effective against EML4-ALK-positive tumors with *ALK* copy number gain mediated by chromothripsis.

DISCUSSION

We obtained the first evidence that chromothripsis is one of the formation mechanisms of *EML4-ALK* rearrangement. Although several groups have observed chromothripsis in various cancers, there is little information on the link between oncogenic fusion genes and chromothripsis. Northcott et al.[16] identified that *PVT1-MYC* and *PVT1-NDRG* arose via chromothripsis in each of two different tumors of medulloblastoma. In addition, Wu et al.[28] found evidence of chromothripsis in a patient-derived prostate tumor with *TMPRSS2-ERG*, which is known as a key fusion gene leading to multigenic events in prostate cancer. Recently, Cazes et al.[29] analyzed the whole genome sequence and reported that the chromosome with *ALK* locus of one neuroblastoma sample was related to the phenomenon of chromothripsis, but this *ALK* fusion was not in-frame. In 2007, Soda et al.[2] provided evidence that it remained undetermined whether the NSCLC

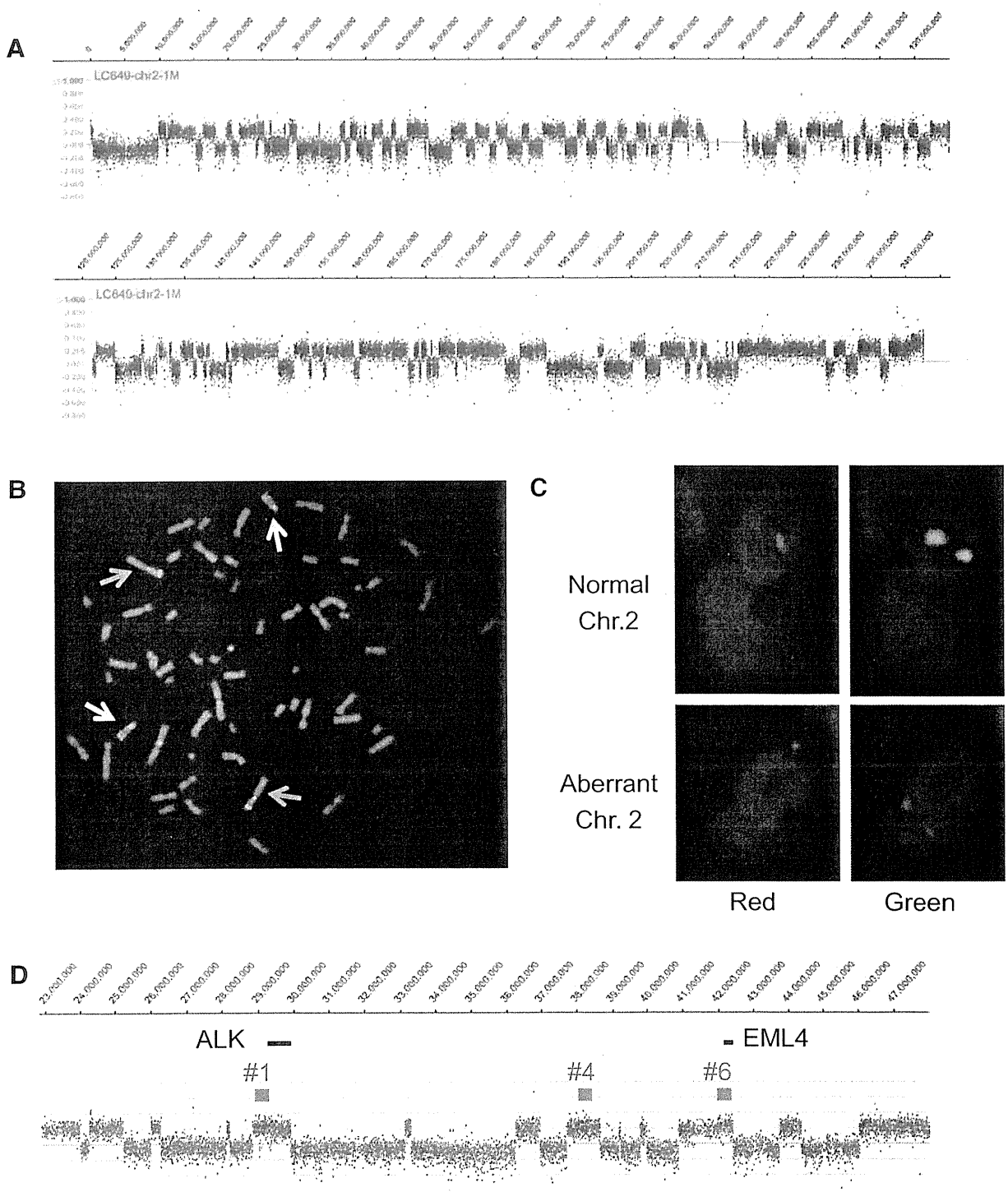

FIGURE 2. Chromosomal structure analysis of JFCR-LC649 cells. *A*, 1M array-based CGH profile of chromosome 2 in JFCR-LC649 cells. An oscillating pattern between two copy number states was observed within chromosome 2 of JFCR-LC649 cells. *B*, FISH analysis of a metaphase chromosome spread in JFCR-LC649 cells using probes of the centromeric region of chromosome 2 (red) and 3′*ALK* (green). JFCR-LC649 cells contained two aberrant chromosome 2 (indicated with yellow arrows) and two normal chromosome 2 (indicated with red arrows). *C*, FISH analysis of a metaphase chromosome spread in JFCR-LC649 cells using the dual color probe set (#1 probe, red; #4 and #6 probes, green). In normal chromosome 2, all signals existed in the same position but in aberrant chromosome 2 the green signal split, indicating fragmentation and scattering of the chromosome had occurred. *D*, Schematic representation of the three kinds of FISH probes (1, 4, and 6).

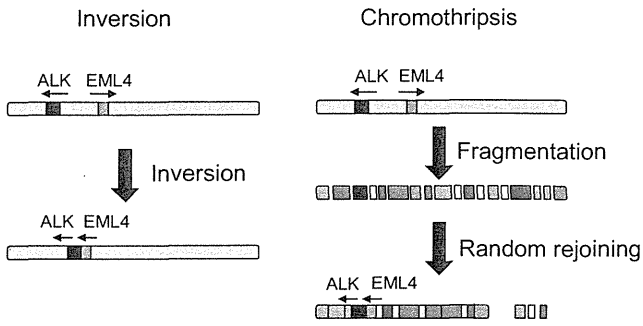

FIGURE 3. Model of *EML4-ALK* rearrangement mediated by inversion and chromothripsis. Chromothripsis causes a one-off catastrophic chromosome breakage and subsequent random reassembly of the chromosome fragments.

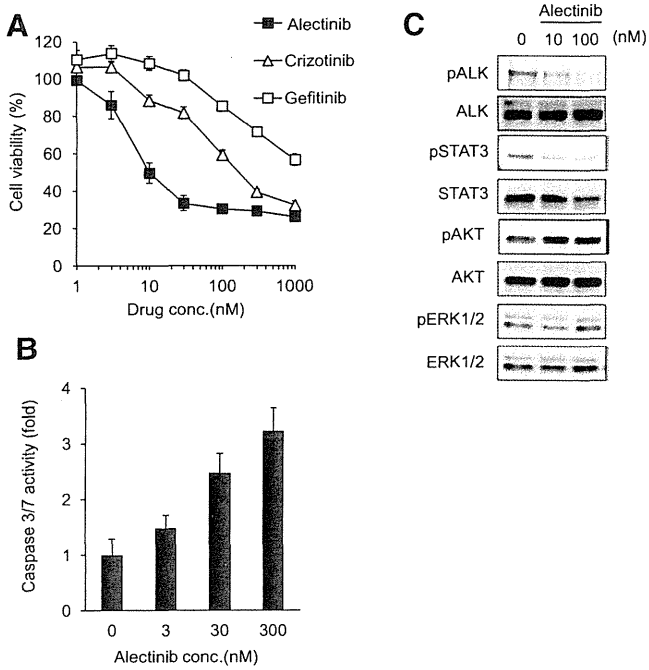

FIGURE 4. Efficacy of ALK inhibitor, alectinib against JFCR-LC649 cells. *A*, Growth inhibition of JFCR-LC649 cells by alectinib. Alectinib and crizotinib both inhibited cell growth of JFCR-LC649. Data are shown as mean ± SD (n = 3 per group). *B*, Increase in caspase 3/7 activity by alectinib in JFCR-LC649 cells. Alectinib induced caspase 3/7 activity of JFCR-LC649 cells in a concentration-dependent manner. Data are shown as mean ± SD (n = 3 per group). *C*, Effect of alectinib on the phosphorylation levels of ALK, STAT3, AKT, and ERK1/2 in JFCR-LC649 cells. Alectinib suppressed phosphorylation of ALK and STAT3 in a concentration-dependent manner but did not suppress phosphorylation of AKT and ERK1/2.

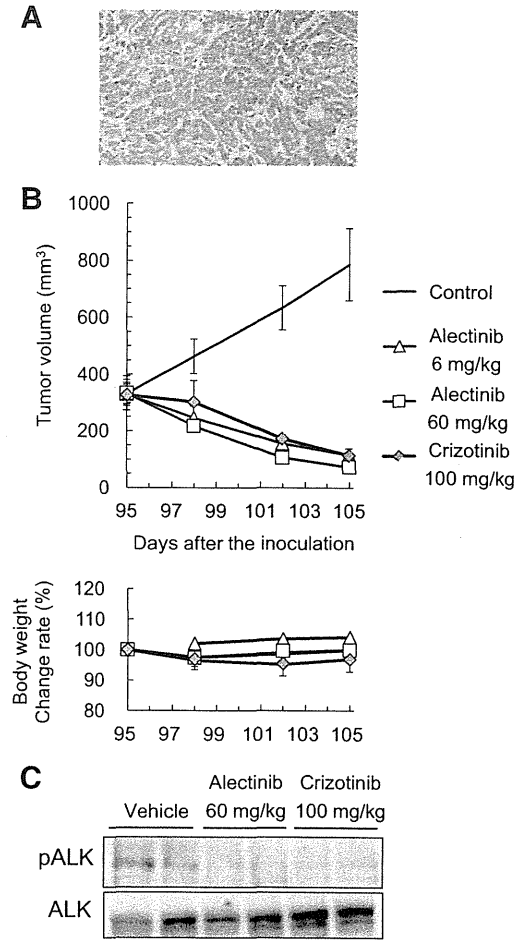

FIGURE 5. Antitumor activity of alectinib or crizotinib against a mouse xenograft model of JFCR-LC649 cells. *A*, JFCR-LC649 xenograft tumors 101 days after inoculation showed ALK-positive IHC staining. *B*, Alectinib or crizotinib once daily for 10 days at the indicated doses reduced the tumor volume without significant body weight change. Data are shown as mean ± SD (n = 4 per group). *C*, Mice bearing JFCR-LC649 cells were orally administered a dose of 0 (vehicle), 60 mg/kg alectinib, or 100 mg/kg crizotinib and the tumors were collected and lysed at 4 hours post-dosing. Both alectinib and crizotinib suppressed phosphorylation of ALK.

cells of a patient with in-frame fusion of *EML4-ALK* harbor a simple inversion within chromosome 2p or whether they contain complex chromosome translocations involving 2p, implying that the mechanism of chromosomal rearrangement in *EML4-ALK* might be complicated. Therefore, we focused on investigating the relationship between *ALK* fusion genes and chromothripsis.

First, we evaluated the array-based CGH copy number profile of chromosome 2 in cell lines harboring *ALK* fusion gene and revealed that JFCR-LC649 cells harbored a chromothripsis-like CGH pattern in chromosome 2 (Fig. 1*D*). We also analyzed EML4-ALK-positive NSCLC cell line NCI-H2228 and NPM-ALK-positive anaplastic large cell lymphoma cell lines, such as KARPAS-299, SR, SUP-M2, L82, and SU-DHL-1, but did not find a chromothripsis-like pattern (Fig. 1*D* and Supplementary Figure S8, Supplemental Digital Content, http://links.lww.com/JTO/A678). Next, to speculate on the occurrence of chromothripsis from the copy number profile in EML4-ALK-positive NSCLC, we analyzed

an array-based CGH data set of five clinical samples derived from EML4-ALK-positive NSCLC patients from The Cancer Genome Atlas (TCGA). Interestingly, only one EML4-ALK-positive case (TCGA-78-7163-11A-01D-2062-01) in TCGA showed a recurrent pattern of chromosomal aberration on the short arm of chromosome 2 (Supplementary Figure S9, Supplemental Digital Content, http://links.lww.com/JTO/A678), suggesting that some EML4-ALK-positive cases might have chromosome 2 mediated by chromothripsis. Thus, chromothripsis might be one of the mechanisms of oncogenic rearrangement of *EML4-ALK* in NSCLC. Further investigation is needed to evaluate the relationship between *EML4-ALK* rearrangement and chromothripsis.

Although several ALK inhibitors, such as crizotinib and alectinib, have demonstrated a clinical benefit against ALK fusion-positive lung adenocarcinoma patients, information on the effectiveness of these ALK inhibitors against other lung cancer subtypes than adenocarcinoma is limited because most ALK fusion-positive patients have adenocarcinoma histology. However, *ALK* rearrangements have also been seen, albeit to a much lesser extent, in other NSCLC.[30,31] The JFCR-LC649 cells we used were established from a surgically resected tumor specimen diagnosed as a rare subtype of NSCLC termed pulmonary pleomorphic carcinoma, which generally shows a poor response to chemotherapy regimens.[32] Histopathologically, a pulmonary pleomorphic carcinoma is defined as a tumor that combines spindle or giant cell carcinoma with any of the more usual patterns of NSCLC,[32] and our case is composed of adenocarcinoma and spindle cell carcinoma. Because we anticipated that we would be able to obtain a distinct cell line derived from the patient with pulmonary pleomorphic carcinoma containing a component of adenocarcinoma, we conducted IHC on mouse xenograft tumors of JFCR-LC649 cells to detect the expression of TTF-1, Napsin A, vimentin, E-cadherin, and p40. As mentioned in the Results section, we found that the xenograft tumors were positive for TTF-1, Napsin A, vimentin, and E-cadherin but negative for p40 (Supplementary Figure S1, Supplemental Digital Content, http://links.lww.com/JTO/A678), indicating that JFCR-LC649 cells were associated with a phenotype characterized by lung adenocarcinoma cells undergoing epithelial–mesenchymal transition. Thus, JFCR-LC649 cells could be used to understand the efficacy of ALK inhibitors against EML4-ALK rearranged pulmonary pleomorphic carcinoma with adenocarcinoma components. Needless to say, the case of JFCR-LC649 is not an exception because the International Association for the Study of Lung Cancer proposes that ALK testing is recommended for adenocarcinomas and mixed lung cancers with an adenocarcinoma component.

Our study also has implications for the EML4-ALK downstream signaling pathway. We confirmed that alectinib was effective against JFCR-LC649 cells harboring EML4-ALK, suppressing phosphorylation of STAT3 but not that of AKT and ERK1/2 in this cell (Fig. 4*B*). In our previous study, however, alectinib suppressed phosphorylation of AKT as well as that of STAT3 but did not suppress that of ERK1/2 in NCI-H2228 cells expressing EML4-ALK.[17] In addition, another ALK inhibitor NVP-TAE684 suppressed phosphorylation of STAT3 but not ERK1/2 in NCI-H2228 cells.[33] However, in EML4-ALK-positive NCI-H3122 cells, both crizotinib and NVP-TAE684 suppressed phosphorylation of STAT3, AKT, and ERK1/2.[25,34] Downstream components of EML4-ALK might depend on cell type; however, further detailed study is needed to evaluate the downstream signal of EML4-ALK.

ACKNOWLEDGMENTS

Parts of this study were supported financially by Grants-in-Aid for Scientific Research from the Ministry of Education, Culture, Sports, Science and Technology, Japan, grants from the Japan Society for the Promotion of Science, the Ministry of Health, Labour and Welfare, and the Princess Takamatsu Cancer Research Fund, and Smoking Research Foundation.

REFERENCES

1. Kantarjian H, Sawyers C, Hochhaus A, et al.; International STI571 CML Study Group. Hematologic and cytogenetic responses to imatinib mesylate in chronic myelogenous leukemia. *N Engl J Med* 2002;346:645–652.
2. Soda M, Choi YL, Enomoto M, et al. Identification of the transforming EML4-ALK fusion gene in non-small-cell lung cancer. *Nature* 2007;448:561–566.
3. Takeuchi K, Soda M, Togashi Y, et al. RET, ROS1 and ALK fusions in lung cancer. *Nat Med* 2012;18:378–381.
4. Kohno T, Ichikawa H, Totoki Y, et al. KIF5B-RET fusions in lung adenocarcinoma. *Nat Med* 2012;18:375–377.
5. Lipson D, Capelletti M, Yelensky R, et al. Identification of new ALK and RET gene fusions from colorectal and lung cancer biopsies. *Nat Med* 2012;18:382–384.
6. Kwak EL, Bang YJ, Camidge DR, et al. Anaplastic lymphoma kinase inhibition in non-small-cell lung cancer. *N Engl J Med* 2010;363:1693–1703.
7. Camidge DR, Bang YJ, Kwak EL, et al. Activity and safety of crizotinib in patients with ALK-positive non-small-cell lung cancer: updated results from a phase 1 study. *Lancet Oncol* 2012;13:1011–1019.
8. Seto T, Kiura K, Nishio M, et al. CH5424802 (RO5424802) for patients with ALK-rearranged advanced non-small-cell lung cancer (AF-001JP study): a single-arm, open-label, phase 1-2 study. *Lancet Oncol* 2013;14:590–598.
9. Ou SH, Bang YJ, Camidge DR, et al. Efficacy and safety of crizotinib in patients with advanced ROS1-rearranged non-small cell lung cancer (NSCLC). *J Clin Oncol* 2013;31 (suppl; abstr 8032).
10. Drilon A, Wang L, Hasanovic A, et al. Response to cabozantinib in patients with RET fusion-positive lung adenocarcinomas. *Cancer Discov* 2013;3:630–635.
11. Stephens PJ, Greenman CD, Fu B, et al. Massive genomic rearrangement acquired in a single catastrophic event during cancer development. *Cell* 2011;144:27–40.
12. Molenaar JJ, Koster J, Zwijnenburg DA, et al. Sequencing of neuroblastoma identifies chromothripsis and defects in neuritogenesis genes. *Nature* 2012;483:589–593.
13. Magrangeas F, Avet-Loiseau H, Munshi NC, Minvielle S. Chromothripsis identifies a rare and aggressive entity among newly diagnosed multiple myeloma patients. *Blood* 2011;118:675–678.
14. Kloosterman WP, Hoogstraat M, Paling O, et al. Chromothripsis is a common mechanism driving genomic rearrangements in primary and metastatic colorectal cancer. *Genome Biol* 2011;12:R103.
15. Rausch T, Jones DT, Zapatka M, et al. Genome sequencing of pediatric medulloblastoma links catastrophic DNA rearrangements with TP53 mutations. *Cell* 2012;148:59–71.
16. Northcott PA, Shih DJ, Peacock J, et al. Subgroup-specific structural variation across 1,000 medulloblastoma genomes. *Nature* 2012;488:49–56.
17. Sakamoto H, Tsukaguchi T, Hiroshima S, et al. CH5424802, a selective ALK inhibitor capable of blocking the resistant gatekeeper mutant. *Cancer Cell* 2011;19:679–690.
18. Kitada K, Aida S, Aikawa S. Coamplification of multiple regions of chromosome 2, including MYCN, in a single patchwork amplicon in cancer cell lines. *Cytogenet Genome Res* 2012;136:30–37.
19. Johansson L. Histopathologic classification of lung cancer: Relevance of cytokeratin and TTF-1 immunophenotyping. *Ann Diagn Pathol* 2004;8:259–267.

20. Bishop JA, Sharma R, Illei PB. Napsin A and thyroid transcription factor-1 expression in carcinomas of the lung, breast, pancreas, colon, kidney, thyroid, and malignant mesothelioma. *Hum Pathol* 2010;41:20–25.
21. Sequist LV, Waltman BA, Dias-Santagata D, et al. Genotypic and histological evolution of lung cancers acquiring resistance to EGFR inhibitors. *Sci Transl Med* 2011;3:75ra26.
22. Devarajan E, Song YH, Krishnappa S, Alt E. Epithelial-mesenchymal transition in breast cancer lines is mediated through PDGF-D released by tissue-resident stem cells. *Int J Cancer* 2012;131:1023–1031.
23. Bishop JA, Teruya-Feldstein J, Westra WH, et al. p40 (DeltaNp63) is superior to p63 for the diagnosis of pulmonary squamous cell carcinoma. *Mod Pathol* 2012;25:405–415.
24. Kitada K, Taima A, Ogasawara K, Metsugi S, Aikawa S. Chromosome-specific segmentation revealed by structural analysis of individually isolated chromosomes. *Genes Chromosomes Cancer* 2011;50:217–227.
25. Katayama R, Khan TM, Benes C, et al. Therapeutic strategies to overcome crizotinib resistance in non-small cell lung cancers harboring the fusion oncogene EML4-ALK. *Proc Natl Acad Sci U S A* 2011;108:7535–7540.
26. Katayama R, Shaw AT, Khan TM, et al. Mechanisms of acquired crizotinib resistance in ALK-rearranged lung Cancers. *Sci Transl Med* 2012;4:120ra17.
27. Kuromitsu S, Mori M, Shimada I, et al. Anti-tumor activity of ASP3026, –A novel and selective ALK inhibitor. *Cancer Res* 2011;71 (suppl; abstr 2821).
28. Wu C, Wyatt AW, McPherson A, et al. Poly-gene fusion transcripts and chromothripsis in prostate cancer. *Genes Chromosomes Cancer* 2012;51:1144–1153.
29. Cazes A, Louis-Brennetot C, Mazot P, et al. Characterization of rearrangements involving the ALK gene reveals a novel truncated form associated with tumor aggressiveness in neuroblastoma. *Cancer Res* 2013;73:195–204.
30. Boland JM, Erdogan S, Vasmatzis G, et al. Anaplastic lymphoma kinase immunoreactivity correlates with ALK gene rearrangement and transcriptional up-regulation in non-small cell lung carcinomas. *Hum Pathol* 2009;40:1152–1158.
31. Gainor JF, Varghese AM, Ou SH, et al. ALK rearrangements are mutually exclusive with mutations in EGFR or KRAS: an analysis of 1,683 patients with non-small cell lung cancer. *Clin Cancer Res* 2013;19:4273–4281.
32. Rossi G, Cavazza A, Sturm N, et al. Pulmonary carcinomas with pleomorphic, sarcomatoid, or sarcomatous elements: a clinicopathologic and immunohistochemical study of 75 cases. *Am J Surg Pathol* 2003;27:311–324.
33. Tanizaki J, Okamoto I, Takezawa K, et al. Combined effect of ALK and MEK inhibitors in EML4-ALK-positive non-small-cell lung cancer cells. *Br J Cancer* 2012;106:763–767.
34. Koivunen JP, Mermel C, Zejnullahu K, et al. EML4-ALK fusion gene and efficacy of an ALK kinase inhibitor in lung cancer. *Clin Cancer Res* 2008;14:4275–4283.

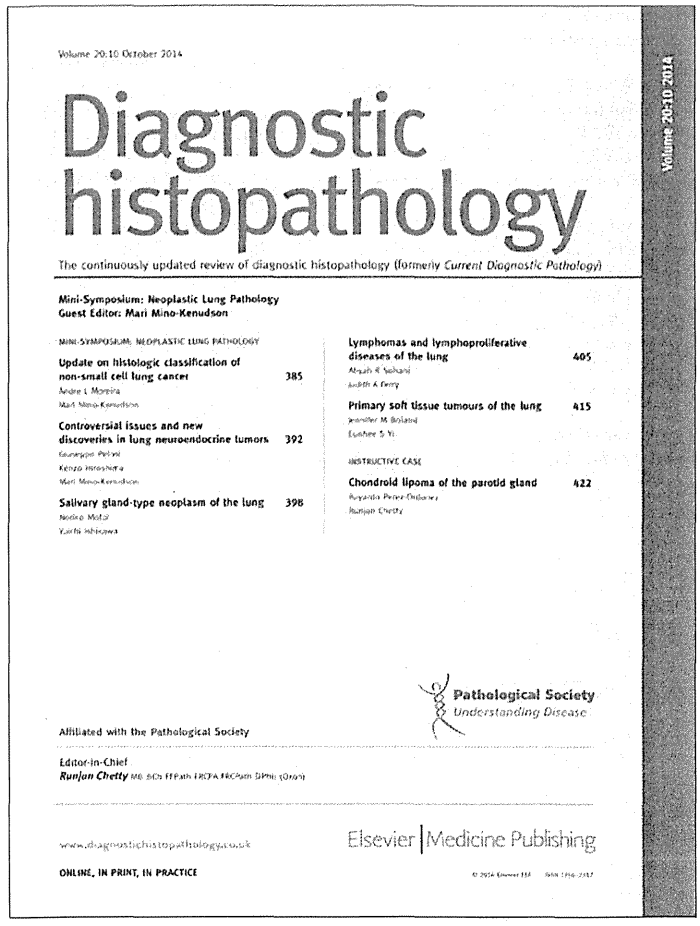

Volume 20:10 October 2014

Diagnostic histopathology

The continuously updated review of diagnostic histopathology (formerly *Current Diagnostic Pathology*)

Volume 20:10 2014

Mini-Symposium: Neoplastic Lung Pathology
Guest Editor: Mari Mino-Kenudson

Pathological Society
Understanding Disease

Affiliated with the Pathological Society

www.diagnostichistopathology.co.uk

Elsevier | Medicine Publishing

ONLINE, IN PRINT, IN PRACTICE

Salivary gland-type neoplasm of the lung

Noriko Motoi
Yuichi Ishikawa

Abstract
Salivary gland-type tumours of the lung, which include adenoid cystic carcinoma and mucoepidermoid carcinoma, are rare entities. Histologically, they show morphologies that are similar to those of salivary gland origin. For classification purposes, the terminology applied to tumours of salivary gland origin is also applied to their pulmonary counterparts. Of these types of tumours, adenoid cystic carcinoma is the most common followed by mucoepidermoid carcinoma. Epithelial-myoepithelial carcinoma and pleomorphic adenoma are uncommon. The possibility of metastasis from the salivary glands is important to exclude through careful examination of patients' medical history because low-grade salivary cancers can metastasize after long latencies. A gene rearrangement analysis is helpful in making a definitive diagnosis, particularly in cases with an unusual morphology. Molecular-based classification may be useful to understand the nature of morphologically varied tumours. The immunohistochemical profile of the tumours is also a valuable tool for an accurate diagnosis in difficult cases.

Keywords adenoid cystic carcinoma; epithelial-myoepithelial carcinoma; lung; mucoepidermoid carcinoma; pleomorphic adenoma; salivary gland-type tumour

Introduction

Salivary gland-type tumours of the lung are a rare type of neoplasm, and submucosal exocrine glands in the central airways are considered to be the origin of such neoplasms. In adults, the vast majority of all tracheal tumours are malignant, while the majority of those are benign in children. Primary tracheal malignant tumours are uncommon, accounting for up to 0.2% of all respiratory malignancy in the United States.[1,2] Of those, squamous cell carcinoma comprises the majority in population-based studies,[1] but in our experience and others based on pathological examinations, adenoid cystic carcinoma (ACC), a salivary gland-type tumour, is equally or more prevalent than squamous cell carcinoma.[2] Among other tumours of exocrine gland origin, mucoepidermoid carcinoma (MEC) is much less common than ACC, but is more prevalent than benign ones in the trachea. Similarly, ACC and MEC are relatively common types of primary salivary gland-type tumours of the bronchus, whereas epithelial-myoepithelial carcinoma (EMC) is very rare and pleomorphic adenoma (PA) or mixed tumour is also very uncommon.[1]

Salivary gland-type tumours of the trachea, main stem or lobar bronchus show the similar histology to those of salivary gland origin. Therefore, the terminology applied to salivary gland tumours is also applied to their lung counterparts. One of the important issues for surgical pathologists is to exclude the possibility of metastasis from major or minor salivary glands, especially when a tumour is encountered in the peripheral lung. Careful examination of the patients' past medical history is recommended because low-grade cancer of salivary gland origin can be indolent with a long time period before metastasis.

The pathological classification of tumours of the salivary glands was extensively revised with many new entities in 2005. The current WHO classification of head and neck tumours (published in 2005) recognizes 24 malignant and 10 benign epithelial tumours.[3,4] Of those, several entities are unique to the salivary glands, such as basal cell adenocarcinoma and polymorphous low-grade adenocarcinoma. In the current WHO classification of lung tumours (published in 2004),[5] only three malignant salivary gland-type tumours, i.e., ACC, MEC and EMC, along with two benign tumours, i.e. mucous gland adenoma and PA are described, reflecting the low prevalence of salivary gland-type tumours in the lung. Since there have been additional insights into the tumours of salivary gland origin even after the publication of the WHO classification of head and neck tumours,[6] the updated criteria and information are also applied to lung counterparts.

For tumours of salivary gland origin, grading is recommended for ACC and MEC but is not recommended for other entities because their diagnoses already reflect the level of malignant potential. For instance, some entities are acknowledged as low-grade malignancy (polymorphous low-grade adenocarcinoma, basal cell adenocarcinoma, acinic cell adenocarcinoma) and others as high-grade malignancy (salivary duct carcinoma).[4] A similar grading system may be applicable to lung counterparts, although there is currently not enough evidence to support its role, given the fact that high-grade MEC is rarely encountered.

Salivary gland-type tumours in general exhibit various morphologies, thus differentiation of one entity from another can be problematic. In such cases, molecular testing, in particular, a gene rearrangement analysis including cytogenetic approach and fluorescence in-situ hybridization (FISH) may be helpful in making a definitive diagnosis. The application of genetic approaches as a basis for classification is still controversial but molecular techniques may help in understanding the nature of morphologically varied tumours. Immunohistochemistry may also be a valuable tool in some diagnostically-challenging cases.

In this review, we will focus on three malignant tumours (ACC, MEC and EMC) and one benign tumour (PA), which are most commonly encountered in the lung, and will describe their cytomorphologic features, immunohistochemical findings and molecular alterations.

Adenoid cystic carcinoma

ACC, one of the most common malignant salivary gland-type tumours in the lung, consists of epithelial and myoepithelial

Noriko Motoi *MD PhD Division of Pathology, The Cancer Institute, Department of Pathology, The Cancer Institute Hospital, Japanese Foundation for Cancer Research (JFCR), Tokyo, Japan. Conflicts of interest: none.*

Yuichi Ishikawa *MD PhD Division of Pathology, The Cancer Institute, Department of Pathology, The Cancer Institute Hospital, Japanese Foundation for Cancer Research (JFCR), Tokyo, Japan. Conflicts of interest: none.*

cells, which show variable morphological configurations including tubular, cribriform and solid patterns. Alternative names are cylindroma and adenocystic carcinoma, although their use is not recommended because of erroneous impression such as natures of a benign tumour or real adenocarcinoma.

ACCs comprise 1% or less of all lung tumours,[7] ranging from 14% to 42% of pulmonary salivary gland-type carcinomas[8,9] with no gender predominance. The average age at presentation is 50 years. ACC does not seem to be associated with tobacco smoking.

Common symptoms of ACC include shortness of breath, coughing, wheezing and haemoptysis due to airway obstruction. Radiologic imaging typically shows a centrally located mass that may have an endobronchial component. When compared to MEC, ACC is larger in size and more frequently involves the central airways, and has a higher median uptake of FDG.[10]

ACC deceptively infiltrates peribronchial soft tissue, insidiously grows, and sometimes extends into the lung parenchyma and mediastinum. Perineural invasion, frequently found in ACC, renders complete surgical resection difficult, and results in relatively frequent local recurrence. Metastases to distant organs are uncommon. It is recommended that the TNM system of lung tumours be used for staging of ACC.

Cytologic findings

ACC is cytologically characterized by three-dimensional microacinar pattern with pale opaque globules corresponding to intraluminal hyalinized or myxoid material. It should be noted that the myxoid matrix is positive not only for PAS, but also for other mucin stains such as alcian blue and mucicarmine. The matrix should also be differentiated from collagen of the basal membrane. The latter is positive for glycogen (that is positive for PAS and negative for PAS/d), but not for mucin.

Macroscopic findings

ACC typically arises as an endobronchial mass within central bronchi or in the trachea. Tumours may show a well-delineated grayish-white, homogeneous cut surface, but frequently infiltrate beyond the visible macroscopic margins. The peribronchial soft tissues and any surgical margins should therefore be extensively sampled and analyzed, both at frozen section and in resection specimens.

Histopathologic findings

ACC consists of small-sized cells with scant cytoplasm and usually small, homogeneous hyperchromatic nuclei that infrequently exhibit mitoses (Figures 1 and 2). The tumour often shows perineural invasion (Figure 3). Characteristic architecture includes cribriform, tubular and solid patterns. The most characteristic cribriform pattern consists of cells surrounding cylinders of connective tissue with variably myxoid and hyalinized material, from which the term "cylindroma" originated (Figure 1). When forming tubules lined by two to three cells, the luminal cells are cuboidal and the peripheral cells form a myoepithelial layer (Figure 2). Both ductal and myoepithelial natures can be demonstrated by their immunoreactivity to cytokeratin, and vimentin, actin and S-100, respectively. Immunohistochemically the matrix, which is positive for type IV collagen, laminin and heparin sulphate, recapitulates basement membrane-like material.

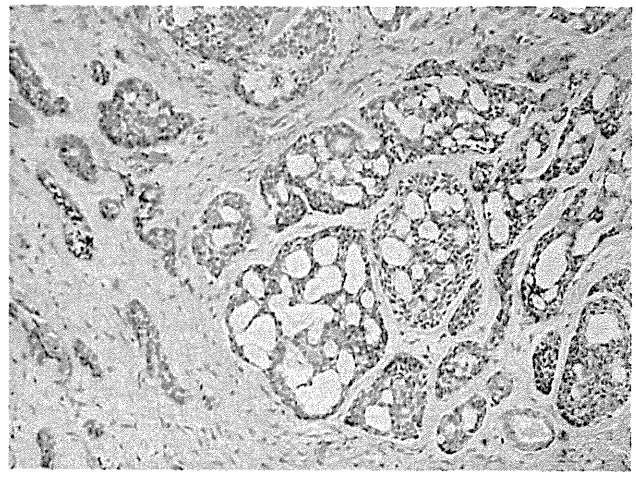

Figure 1 Adenoid cystic carcinoma showing a cribriform pattern and characteristic eosinophilic cylinders.

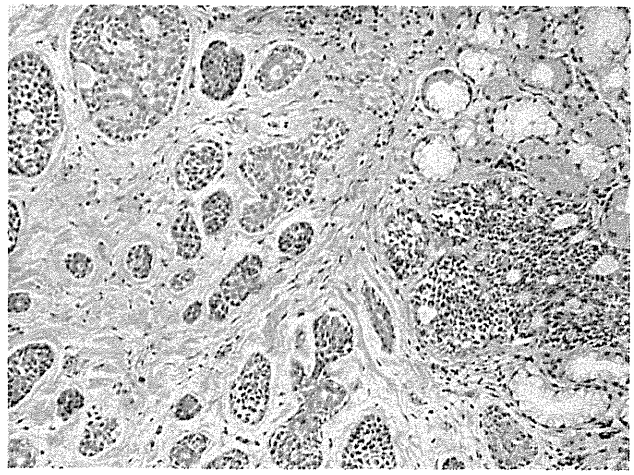

Figure 2 Adenoid cystic carcinoma showing a tubular pattern with inner and outer layers, involving bronchial glands.

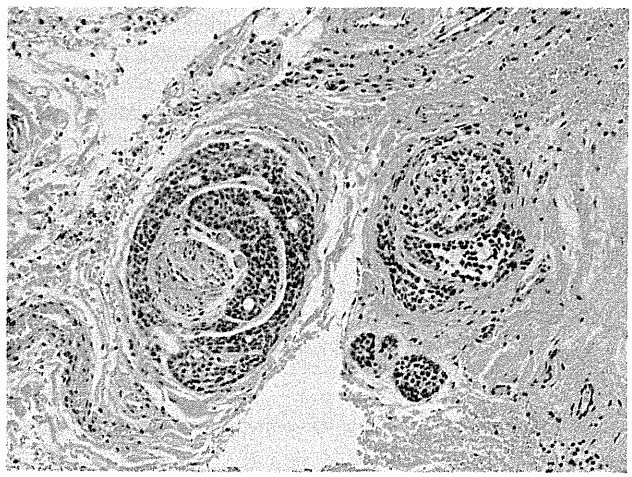

Figure 3 Perineural invasion is frequent in adenoid cystic carcinoma.

The differential diagnosis of ACC includes carcinoid tumours, basaloid carcinoma and small cell carcinoma, all of which can typically be distinguished by immunohistochemistry. In contrast to ACC, basaloid carcinoma commonly has a high proliferation rate. In addition, PA with a focal cribriform architecture may resemble ACC. Metastasis from other organs should be carefully ruled out.[11]

Genetic profile

A fusion of *MYB* oncogene and *NFIB* transcription factor was reported in 30–100% of ACCs of the head and neck and breast,[12,13] but there has been no report for bronchopulmonary counterparts to date. Given its scarcity, no large-scale molecular studies have been performed in ACC of the lung. Loss of heterozygosity of chromosomes 3p14 and 9p was reported in two tumours examined.[14] High-resolution CGH analysis performed in two ACCs of the main bronchus showed losses at 3p, 4p and 15q, and gains at 12q15 (*MDM2* site).[15] *EGFR* and *RAS* mutations were not identified.[16,17] Despite immunoreactivity to KIT seen in the majority of ACCs, *KIT* mutations are absent.[17,18] Whereas whole-exome sequencing of the head and neck ACC identified mutations in *PIK3CA*, *ATM*, *CDKN2A*, *SF3B1*, *SUFU*, *TSC1*, *CYLD*, *NOTCH1/2*, *SPEN* and *FGFR2*,[19] no similar studies have been conducted in bronchopulmonary ACC.

Prognosis and prognostic factors

ACC typically follows an indolent clinical course in which local, often multiple, recurrences may occur over a period of 10–15 years following resection. Distant metastases may eventually occur. Advanced tumour stage at diagnosis, the presence of positive margins at surgery and a solid growth pattern are associated with unfavourable patient outcomes.

Mucoepidermoid carcinoma

Although rare, MEC is one of the most common salivary gland-type tumours arising in the trachea and bronchi. MEC comprises mucin-secreting cells, non-keratinsing squamoid cells and intermediate cells. MEC is classified as low-grade and high-grade, based on histological criteria.

MEC accounts for less than 1% of lung carcinoma and 54–78% of pulmonary salivary gland-type carcinoma without apparent gender predominance. MEC presents between the first and the 8th decade, with a mean age of 30–40 years. Fifty percent of tumours occur in individuals under 30 years of age. Tobacco smoking does not seem to be a risk factor for MEC.

Clinical manifestations include wheezing, coughing, haemoptysis, and obstructive pneumonia, though some patients are asymptomatic. CT imaging shows a well-defined endobronchial mass located in the central airway. By PET imaging, MEC is usually FDG-avid.[20] Both low-grade and high-grade MEC may involve lymph nodes, either by direct extension or via lymphatic invasion, which is more common in high-grade lesions. It is recommended that the TNM system of lung tumours be used for staging of MEC as well.

Cytological findings

Three cell types are observed to various extent: glandular cells with eccentric nuclei, delicate cytoplasm and unclear cell borders; intermediate cells with even chromatin, and small, round, and uniform nuclei, showing sheet-like arrangement; and squamoid cells with a dense cytoplasm and clear cell borders.

Macroscopic findings

MEC is a well-circumscribed soft mass that typically arises as an endobronchial mass in the central airway (Figure 4), measuring 3 cm on average (ranging from 1 to 8 cm), and showing a grey-white to pink-tan and sometimes mucinous and cystic cut surface. High-grade tumours are usually more infiltrative, showing an ill-defined mass.

Histopathological findings

MEC is composed of three different types of cells. They are glandular, squamoid and intermediate cells and are mixed to various degrees (Figures 5 and 6).

A subclassification into low-grade and high-grade types has been employed. Low-grade tumours comprise three cell types, including mucus-secreting, squamous (or squamoid) and intermediate cells, and often show cystic patterns with solid areas. Tumour islands contain both cystic and solid patterns. The cystic components consist of cytologically bland columnar cells with mucin and rare mitoses. Solid components composed of squamoid and/or intermediate cells typically surround the cystic areas. Intermediate cells are oval or polygonal with round nuclei, eosinophilic or clear cytoplasm and rare necrosis. Stromal calcification and ossification, often with a granulomatous reaction, may be seen around areas of mucus extravasation.

High-grade MECs are more infiltrative than low-grade ones and are mainly composed of atypical squamoid and intermediate cells, with frequent mitosis and necrosis, accompanied by variable numbers of mucin-secreting cells. Primary high-grade tumours are rare and the diagnosis should be made after careful exclusion of adenosquamous carcinoma. The features favouring high-grade MEC over adenosquamous cell carcinoma include: (i) exophytic endobronchial growth; (ii) surface epithelium lacking the changes of in-situ carcinoma; (iii) absence of cellular keratinization and squamous pearl formation; and (iv) background low-grade MEC. The lack of TTF-1 and Napsin A expression in MEC may also be useful for establishing the diagnosis.[21,22] Rearrangement of the mammalian mastermind-like

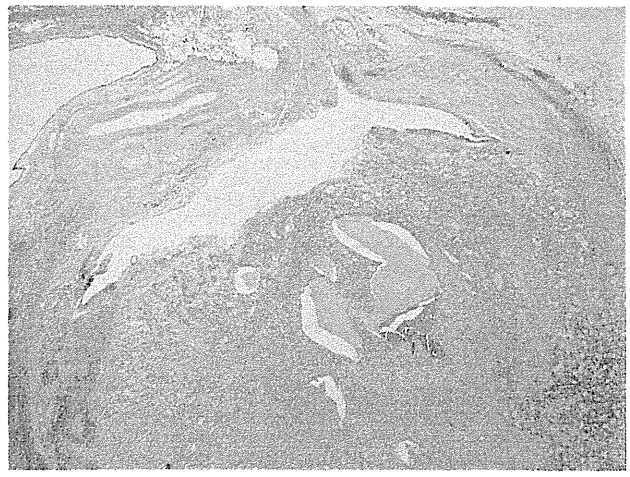

Figure 4 Mucoepidermoid carcinoma protruding in a broncheal lumen.

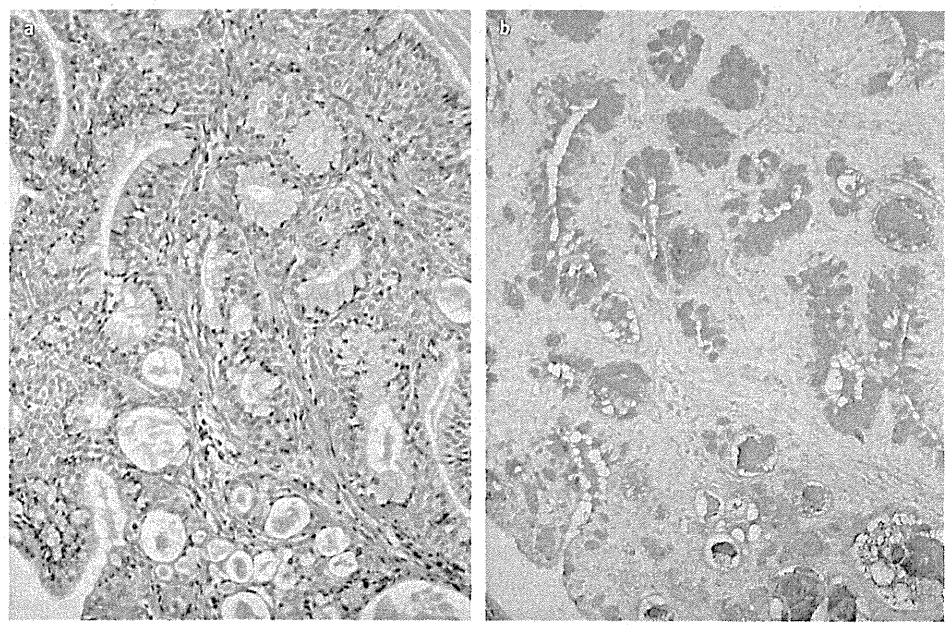

Figure 5 Mucoepidermoid carcinoma composed of mucinous cells and surrounding squamoid cells as well as intermediate cells (**a**). Alcian-blue stain highlights the mucinous cells (**b**).

2 (*MAML2*) gene is observed exclusively in MEC.[23] However, high-grade MEC may not be reliably distinguished from adenosquamous carcinoma of the lung.[24]

Genetic profile

CRTC1-MAML2 rearrangements occur in both low-grade and high-grade MECs, but more frequently in low-grade tumours (Figure 7), and they are also found in salivary gland counterparts.[25] The *CRTC1-MAML2* rearrangement may potentially serve as an important diagnostic marker, particularly in differentiating MEC from adenosquamous carcinoma. Additionally, *EGFR* mutations have been reported in some cases, but their significance is unclear in terms of diagnosis and therapy.[26]

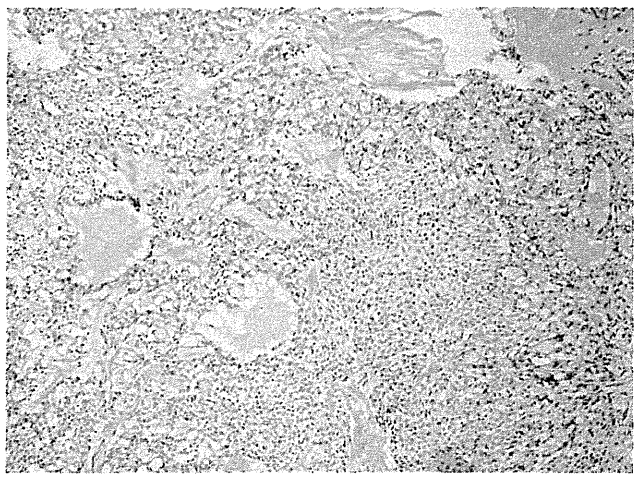

Figure 6 Mucoepidermoid carcinoma showing proliferation of intermediate cells and occasional glands with mucin.

Prognosis and prognostic factors

Low-grade MECs have favourable outcomes, whereas high-grade MECs behave similarly to non-small cell carcinomas. Adverse prognostic factors include positive resection margins and lymph node metastasis.

Epithelial-myoepithelial carcinoma

EMC is a malignant tumour showing variable compositions of two cell types, which typically form duct-like structures. The biphasic morphology is characterized by an inner layer of duct lining composed of epithelial-type cells and an outer layer of clear, myoepithelial-type cells forming and clear, myoepithelial-type cells. Before the introduction of the term EMC, these tumours were often called as adenomyoepithelioma.

EMC is a very rare tumour, with less than 60 reported cases in the English literature.[8,27–29] EMC represents approximately 4–8% of the salivary gland-type tumours of the lung[8,9] with no gender preference. The ages of the patients range from 33 to 71 years. EMC develops mostly in the trachea or main bronchus, but also in the peripheral lung. Patients with EMC experience symptoms related to airway obstruction such as coughing, voice change, chest discomfort and dyspnoea, sometimes asthma-like symptoms, as well as fever. Some patients may not have any presenting symptoms.

Macroscopic findings

EMC appears typically as a solid, polypoid or dome-shaped, endobronchial tumour. The cut surface has a yellow-white or white gelatinous appearance, depending on the proportion of tumour cell components.[27] Tumour size ranges from 0.7 to 5.5 cm.

Histopathological findings

EMC has a lobulated growth pattern with a mixed tubular and solid architecture. The hallmark of its histology is the presence of

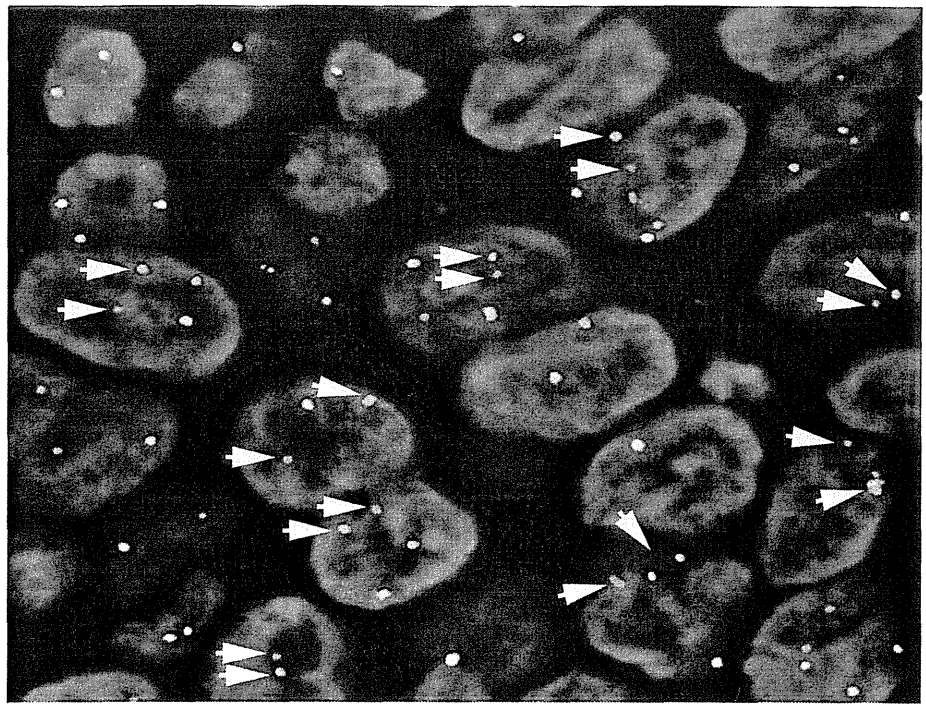

Figure 7 An example of mucoepidermoid carcinoma harbouring a *MAML2* gene rearrangement. *MAML2* FISH demonstrating multiple pairs of red and green signals that are separated (split signals, arrows) consistent with gene rearrangement (Courtesy of Dr. Sanja Dacic).

double-layered duct-like structures similar to that of the salivary gland.[3] The inner layer is formed by a single row of cuboidal cells with dense, finely granular cytoplasm and central or basal, round nuclei. The outer layer may show single or multiple layers of polygonal cells, with well-defined borders; the cytoplasm is typically clear and nuclei are vesicular and slightly eccentric. The duct-like structures are usually surrounded by PAS-positive, hyaline, eosinophilic strands of basement membrane-like substance. Papillary-cystic areas usually exhibit the double-layered pattern, but solid-tumour areas may be exclusively formed by clear cells. Some EMC show necrosis. Cytological atypia can be observed in some cases. Zero to 80 mitoses per 10 HPF can be identified in EMC.

Immunohistochemical profile

The clear cell components are immunoreactive to myoepithelial markers (alpha-smooth muscle actin, HHF-35, p63 and/or calponin), and are negative for CD10 and high-molecular weight cytokeratin, which are positive in clear cell renal cell carcinoma, and thyroglobulin, which is positive in thyroid cancer. The luminal cells stain positively with cytokeratins.

Genetic profile

A limited number of EMC of salivary gland origin has been karyotyped, half of them showing non-distinct chromosomal alterations and the remaining normal karyotypes. No recurrent abnormalities have been identified; however, no such studies have been conducted in EMC of the lung. Interestingly, the association of malignant potential of EMC and the cytoplasmic localization of p27 in myoepithelial tumour cells has been reported, but is subject to concern and debate.[30]

Prognosis and prognostic factors

EMC is considered to be a low-grade malignant tumour, and most resectable EMCs can be cured by complete surgical resection. Positive margins are associated with local recurrence, which occurs in approximately 23–80% of the resected cases, and metastasis may be seen in 14–25%. The most common metastatic sites are regional lymph nodes, and rarely the liver, lung and soft tissue. Lack of recognized histopathological features of malignancy, such as mitotic activity of no more than 1/20 HPF and an absence of necrosis correlate well with lack of nodal involvement and favourable patient outcomes. Some EMCs that developed recurrence and/or metastasis had shown higher mitotic rates, necrosis, and cytological atypia. The association of poor prognosis with mitotic activity is also evident in breast, skin and salivary gland counterparts.[27,29,30]

Pleomorphic adenoma (mixed tumour)

PA, also known as mixed tumour, is a benign tumour composed of epithelial and myoepithelial cells, with a myxoid stroma, and is microscopically characterized by architectural, rather than cellular, pleomorphism. Epithelial and modified myoepithelial elements are most commonly intermingled with mucoid, myxoid or chondroid tissue.

PA is a very uncommon salivary gland-type tumour of the lung while it is relatively common in the salivary glands. Most PAs are benign, and rarely show malignant transformation. "Carcinoma ex pleomorphic adenoma" (malignant mixed tumour) is extremely rare in the lung, and only very few cases have been reported. PA of the lung generally originates from the bronchial glands. PA occurs mostly in the trachea or main bronchus.[1,4,5]

PA is usually a slow-growing mass. Small tumours typically form smooth, mobile, firm lumps whereas larger tumours tend to become lobulated and may attenuate the overlying mucosa. PA is typically a solitary lesion though it may be detected coincidentally with other tumours. PA may produce symptoms and signs related to airway obstruction, but patients may also asymptomatic.[1,4,5]

Macroscopic findings

PA tends to form a polypoid tumour in the main bronchus or trachea, demonstrating a well-defined, ovoid or round mass. It is often encapsulated but the capsule varies in thickness and may be partially or completely absent. The cut surface is typically homogeneous and white or tan. It may be glistering if cartilaginous or myxochondroid areas are present. There may also be areas of haemorrhage or necrosis.[4,5]

Histopathological findings

PA of the lung shows a remarkable degree of morphological diversity, similar to that of the salivary gland. The essential components are the capsule, epithelial and myoepithelial cells, and mesenchymal or stromal elements. The capsule varies in thickness and may even be absent. In bronchial or tracheal PA, the capsule may be virtually absent and the tumour abuts onto adjacent structures, such as cartilaginous tissues and non-tumour glands. The characteristics of the epithelial, myoepithelial and stromal components are by and large similar to the salivary gland counterparts. The differential diagnosis includes cellular and solid variant of ACC, EMC, chondroma and hamartoma.[4,5]

Immunohistochemical profile

The epithelial cells are positive for luminal cell markers, such as low molecular weight cytokeratins (CK8, 18, 19), EMA and CEA. The neoplastic myoepithelial cells co-express vimentin and pan-cytokeratin, high-molecular weight cytokeratin and are variably positive for S-100, alpha-smooth muscle actin, GFAP, calponin, CD10 and muscle-specific actin (HHF-35).[6]

Genetic profile

For PA of lung origin, no detailed cytogenetic analysis has been reported. For PA of salivary origin, chromosomal abnormalities are detected approximately 70% of cases with many variants. Of those, 8q12 and 12q13-15 are the commonly involved loci. t(3;8)(p21;q12), t(5;8)(p13;q12), t(9;12)(p24;q14-15) or ins(9;12)(p24;q15) are the most frequent rearrangements.[31]

The target gene located in the 8q12 region has been identified as *PLAG1* in PA of salivary gland origin. The observed fusion genes are *CTNNB1-PLAG1*, *LIFR-PLAG1*, and *SII-PLAG1*. The PLAG1 protein is a nuclear oncoprotein that functions as a DNA-binding transcription factor. Deregulation of the PLAG1 target genes, including *IGF2*, is likely to play a major role in the genesis of PA. The target gene located in the 12q14-15 region has been identified as the high mobility group protein gene, *HMGA2* (also known as *HMGIC*). Two fusion genes, *HMGA2-NFIB* and *HMGA2-FHIT*, have been reported. High-level expression of *HMGA2* resulting from gene amplification may be involved in malignant transformation of PA.[31,32] In the lung counterparts, no gene fusion has been reported to date.

Prognosis and prognostic factors

Although PA is a benign tumour, it can be clinically problematic due to its tendency to recur and risk of malignant transformation, especially in PA of salivary gland origin. In PA of lung origin, however, malignant transformation is extremely rare.[1,4,5] ◆

REFERENCES

1 Gaissert HA, Mark EJ. Tracheobronchial gland tumors. *Cancer Control* 2006; **13:** 286–94.
2 Honings J, Gaissert HA, van der Heijden HF, Verhagen AF, Kaanders JH, Marres HA. Clinical aspects and treatment of primary tracheal malignancies. *Acta Otolaryngol* 2010; **130:** 763–72.
3 Barnes L, Eveson JW, Reichart P, Sidransky D. Pathology and genetics of head and neck tumours. Lyon, France: IARC Press, 2005.
4 Zarbo RJ. Salivary gland neoplasia: a review for the practicing pathologist. *Mod Pathol* 2002; **15:** 298–323.
5 Travis WD, Brambilla E, Mueller-Hermelink K, Harris CC. Pathology and genetics of tumours of the lung, pleura, thymus and heart. Lyon, France: IARC Press, 2004.
6 Nagao T, Sato E, Inoue R, et al. Immunohistochemical analysis of salivary gland tumors: application for surgical pathology practice. *Acta Histochem Cytochem* 2012; **45:** 269–82.
7 Bennett AK, Mills SE, Wick MR. Salivary-type neoplasms of the breast and lung. *Semin Diagn Pathol* 2003; **20:** 279–304.
8 Kang DY, Yoon YS, Kim HK, et al. Primary salivary gland-type lung cancer: surgical outcomes. *Lung Cancer* 2011; **72:** 250–4.
9 Zhu F, Liu Z, Hou Y, et al. Primary salivary gland-type lung cancer: clinicopathological analysis of 88 cases from China. *J Thorac Oncol* 2013; **8:** 1578–84.
10 Elnayal A, Moran CA, Fox PS, Mawlawi O, Swisher SG, Marom EM. Primary salivary gland-type lung cancer: imaging and clinical predictors of outcome. *AJR Am J Roentgenol* 2013; **201:** W57–63.
11 Maziak DE, Todd TR, Keshavjee SH, Winton TL, Van Nostrand P, Pearson FG. Adenoid cystic carcinoma of the airway: thirty-two-year experience. *J Thorac Cardiovasc Surg* 1996; **112:** 1522–31. discussion 1531–1522.
12 Mitani Y, Rao PH, Futreal PA, et al. Novel chromosomal rearrangements and break points at the t(6;9) in salivary adenoid cystic carcinoma: association with MYB-NFIB chimeric fusion, MYB expression, and clinical outcome. *Clin Cancer Res* 2011; **17:** 7003–14.
13 Persson M, Andren Y, Mark J, Horlings HM, Persson F, Stenman G. Recurrent fusion of MYB and NFIB transcription factor genes in carcinomas of the breast and head and neck. *Proc Natl Acad Sci U S A* 2009; **106:** 18740–4.
14 Sugio K, Osaki T, Oyama T, et al. Genetic alteration in carcinoid tumors of the lung. *Ann Thorac Cardiovasc Surg* 2003; **9:** 149–54.
15 Bernheim A, Toujani S, Saulnier P, et al. High-resolution array comparative genomic hybridization analysis of human bronchial and salivary adenoid cystic carcinoma. *Lab Invest* 2008; **88:** 464–73.
16 Macarenco RS, Uphoff TS, Gilmer HF, et al. Salivary gland-type lung carcinomas: an EGFR immunohistochemical, molecular genetic, and mutational analysis study. *Mod Pathol* 2008; **21:** 1168–75.
17 Wetterskog D, Wilkerson PM, Rodrigues DN, et al. Mutation profiling of adenoid cystic carcinomas from multiple anatomical sites identifies mutations in the RAS pathway, but no KIT mutations. *Histopathology* 2013; **62:** 543–50.

18 Aubry MC, Heinrich MC, Molina J, et al. Primary adenoid cystic carcinoma of the lung: absence of KIT mutations. *Cancer* 2007; **110:** 2507–10.

19 Stephens PJ, Davies HR, Mitani Y, et al. Whole exome sequencing of adenoid cystic carcinoma. *J Clin Invest* 2013; **123:** 2965–8.

20 Li X, Zhang W, Wu X, Sun C, Chen M, Zeng Q. Mucoepidermoid carcinoma of the lung: common findings and unusual appearances on CT. *Clin Imaging* 2012; **36:** 8–13.

21 Roden AC, Garcia JJ, Wehrs RN, et al. Histopathologic, immunophenotypic and cytogenetic features of pulmonary mucoepidermoid carcinoma. *Mod Pathol* 2014 Apr 18; http://dx.doi.org/10.1038/modpathol.2014.72 [Epub ahead of print].

22 Shilo K, Foss RD, Franks TJ, DePeralta-Venturina M, Travis WD. Pulmonary mucoepidermoid carcinoma with prominent tumor-associated lymphoid proliferation. *Am J Surg Pathol* 2005; **29:** 407–11.

23 Achcar RDOD, Nikiforova MN, Dacic S, Nicholson AG, Yousem SA. Mammalian mastermind like 2 11q21 gene rearrangement in bronchopulmonary mucoepidermoid carcinoma. *Hum Pathol* 2009; **40:** 854–60.

24 Lantuejoul S, Fior-Gozlan M, Ferretti GR, Moro-Sibilot D. Large cell carcinoma and adenosquamous carcinoma of the lung. In: Hasleton P, Flieder DB, eds. Spencer's pathology of the lung. 6th edn. New York: Cambridge University Press, 2013; 1114–26.

25 O'Neill ID. t(11;19) translocation and CRTC1-MAML2 fusion oncogene in mucoepidermoid carcinoma. *Oral Oncol* 2009; **45:** 2–9.

26 O'Neill ID. Gefitinib as targeted therapy for mucoepidermoid carcinoma of the lung: possible significance of CRTC1-MAML2 oncogene. *Lung Cancer* 2009; **64:** 129–30.

27 Fulford LG, Kamata Y, Okudera K, et al. Epithelial-myoepithelial carcinomas of the bronchus. *Am J Surg Pathol* 2001; **25:** 1508–14.

28 Konoglou M, Cheva A, Zarogoulidis P, et al. Epithelial-myoepithelial carcinoma of the trachea-a rare entity case report. *J Thorac Dis* 2014; **6**(suppl 1): S194–9.

29 Nguyen CV, Suster S, Moran CA. Pulmonary epithelial-myoepithelial carcinoma: a clinicopathologic and immunohistochemical study of 5 cases. *Hum Pathol* 2009; **40:** 366–73.

30 Song DH, Choi IH, Ha SY, et al. Epithelial-myoepthelial carcinoma of the tracheobronchial tree: the prognostic role of myoepithelial cells. *Lung Cancer* 2014; **83:** 416–9.

31 Weinreb I. Translocation-associated salivary gland tumors: a review and update. *Adv Anat Pathol* 2013; **20:** 367–77.

32 Bahrami A, Perez-Ordonez B, Dalton JD, Weinreb I. An analysis of PLAG1 and HMGA2 rearrangements in salivary duct carcinoma and examination of the role of precursor lesions. *Histopathology* 2013; **63:** 250–62.

European Journal of Cardio-Thoracic Surgery Advance Access published January 28, 2014

European Journal of Cardio-Thoracic Surgery (2014) 1-6
doi:10.1093/ejcts/ezt645

ORIGINAL ARTICLE

THORACIC

Segmentectomy for clinical stage IA lung adenocarcinoma showing solid dominance on radiology

Yasuhiro Tsutani[a], Yoshihiro Miyata[a], Haruhiko Nakayama[b], Sakae Okumura[c], Shuji Adachi[d], Masahiro Yoshimura[e] and Morihito Okada[a,*]

[a] Department of Surgical Oncology, Hiroshima University, Hiroshima, Japan
[b] Department of Thoracic Surgery, Kanagawa Cancer Center, Yokohama, Japan
[c] Department of Thoracic Surgery, Cancer Institute Hospital, Tokyo, Japan
[d] Department of Radiology, Hyogo Cancer Center, Akashi, Japan
[e] Department of Thoracic Surgery, Hyogo Cancer Center, Akashi, Japan

* Corresponding author. Department of Surgical Oncology, Research Institute for Radiation Biology and Medicine, Hiroshima University, 1-2-3-Kasumi, Minami-ku, Hiroshima City, Hiroshima 734-0037, Japan. Tel: +81-82-2575869; fax: +81-82-2567109; e-mail: morihito@hiroshima-u.ac.jp (M. Okada).

Received 18 October 2013; received in revised form 3 December 2013; accepted 11 December 2013

Abstract

OBJECTIVES: This study aimed to compare prognosis after segmentectomy and after lobectomy for radiologically determined solid-dominant clinical stage IA lung adenocarcinoma.

METHODS: From a multicentre database of 610 consecutive patients with clinical stage IA lung adenocarcinoma who underwent complete resection after preoperative high-resolution computed tomography (HRCT) and F-18-fluorodeoxyglucose positron emission tomography/computed tomography (FDG-PET/CT), 327 patients with a radiologically determined solid-dominant tumour (solid component on HRCT ≥50%) who underwent lobectomy ($n = 286$) or segmentectomy ($n = 41$) were included.

RESULTS: No significant difference existed in recurrence-free survival (RFS) between the lobectomy and segmentectomy groups (3-year RFS, 84.4 vs 84.8%, respectively; $P = 0.69$). There was no significant difference in recurrence pattern between these two groups (local, 5.6 vs 7.3%, $P = 0.72$; distant, 9.1 vs 4.9%, $P = 0.55$, respectively). Even in patients with pure solid tumours, no significant difference was observed in RFS between lobectomy and segmentectomy groups (3-year RFS, 76.8 vs 84.7%, respectively; $P = 0.48$), as well as in those with a mixed ground-glass opacity tumour (3-year RFS, 91.0 vs 85.0%, respectively; $P = 0.60$). Multivariate Cox analysis demonstrated that solid tumour size on HRCT ($P = 0.048$) and maximum standardized uptake value (SUVmax) on FDG-PET/CT ($P < 0.001$), not the surgical procedure ($P = 0.40$), were independent prognostic factors for RFS.

CONCLUSIONS: RFS depends on solid tumour size on HRCT and SUVmax on FDG-PET/CT, rather than on the surgical procedure, in patients with radiologically detected solid-dominant clinical stage IA lung adenocarcinoma. Patient prognosis is similar after lobectomy and after segmentectomy for solid-dominant tumour.

Keywords: Lung cancer surgery • Positron emission tomography • Computed tomography

INTRODUCTION

Sublobar resection for small-sized non-small-cell lung cancer (NSCLC) has been a topic of debate for a long time [1-6]. Ground-glass opacity (GGO)-dominant early lung adenocarcinomas are thought to be relatively benign [7-9] and can be treated with sublobar resection, including segmentectomy or wedge resection, because these tumours seldom lead to lymph node metastasis [9]. On the other hand, radiologically determined solid-dominant NSCLCs show a more malignant potential, such as pathological invasiveness and lymph node metastasis, than GGO-dominant tumours [8]. Wedge resection, which cannot be used to approach hilar lymph nodes, is inappropriate as a radical procedure for a solid-dominant tumour because such a tumour might have metastasized to lymph nodes. On the other hand, segmentectomy can be used to approach hilar lymph nodes and may be applied to a solid-dominant tumour with ample surgical margin. At present, segmentectomy for a solid-dominant tumour as a radical procedure is controversial. The purpose of this study is to evaluate and compare the prognosis after segmentectomy with that after lobectomy in patients with radiologically assessed solid-dominant clinical stage IA lung adenocarcinoma.

PATIENTS AND METHODS

Patients

We enrolled 610 patients with clinical T1N0M0 stage IA lung adenocarcinoma from four institutions (Hiroshima University, Kanagawa Cancer Center, Cancer Institute Hospital, and Hyogo